### Title

Nuclear factor one B regulates neural stem cell differentiation and axonal projection of corticofugal neurons




### Journal

The Journal of Comparative Neurology, 522(1)

### ISSN

1550-7149



### Authors

Betancourt, Jennifer
Katzman, Sol
Chen, Bin



### Publication Date

2014

### DOI

10.1002/cne.23373

Peer reviewed

Published in final edited form as:
*J Comp Neurol*. 2014 January 1; 522(1): 6–35. doi:10.1002/cne.23373.

# Nuclear Factor One B regulates neural stem cell differentiation and axonal projection of corticofugal neurons

**Jennifer Betancourt**[1], **Sol Katzman**[2], and **Bin Chen**[1,*,#]

[1]Department of Molecular, Cell and Developmental Biology, University of California, Santa Cruz, CA 95064

[2]Center for Biomolecular Science and Engineering, University of California, Santa Cruz, CA 95064

## Abstract

During development of the cerebral cortex, neural stem cells divide to expand the progenitor pool and generate basal progenitors, outer radial glia and cortical neurons. As these newly born neurons differentiate, they must properly migrate toward their final destination in the cortical plate, project axons to appropriate targets, and develop dendrites. However, a complete understanding of the precise genetic mechanisms regulating these steps is lacking. Here we show that a member of the nuclear factor one (NFI) family of transcription factors, NFIB, is essential for many of these processes in mice. We performed a detailed analysis of NFIB expression during cortical development, and investigated defects in cortical neurogenesis, neuronal migration and differentiation in *NfiB*$^{-/-}$ brains. We found that NFIB is strongly expressed in radial glia and corticofugal neurons throughout cortical development. However, in *NfiB*$^{-/-}$ cortices, radial glia failed to generate outer radial glia, subsequently resulting in a loss of late basal progenitors. In addition, corticofugal neurons showed a severe loss of axonal projections, while late-born cortical neurons displayed defects in migration and ectopically expressed the early-born neuronal marker, CTIP2. Furthermore, gene expression analysis, by RNA-sequencing, revealed a misexpression of genes that regulate the cell cycle, neuronal differentiation and migration in *NfiB*$^{-/-}$ brains. Together these results demonstrate the critical functions of NFIB in regulating cortical development.

### Keywords

NFIB; radial glia; outer radial glia; basal progenitors; neuronal migration; neurogenesis

[*]Corresponding Author: Bin Chen, Department of Molecular, Cell and Developmental Biology, University of California, Santa Cruz, 1156 High Street, Santa Cruz, CA 95064, Phone: 8314592630, Fax: 8314593139, bchen@ucsc.edu.

[#]Support Information: This work was funded by R01MH094589 from National Institute of Health (to BC) and a New Faculty Award RN1-00530-1 from California Institute of Regenerative Medicine (to BC). J. B. was supported by training grant R25GM058903 from National Institute of Health.

**Conflict of interest statement**

The authors declare no conflict of interest in the present study.

**Role of authors**

All authors had full access to all the data in the study and take responsibility for the integrity of the data and the accuracy of the data analysis. Study concept and design: JB and BC. Acquisition of data: JB and SK. Analysis and interpretation of data: JB, SK and BC. Drafting of the manuscript: JB, SK and BC. Critical revision of the manuscript for important intellectual content: BC. Statistical analysis: JB and SK. Obtained funding: JB and BC. Administrative, technical and material support: BC. Study supervision: BC.

## Introduction

The mammalian cerebral cortex is a six-layered structure, responsible for higher cognitive function and sensory perception. It is composed of many different neuronal subtypes, each with unique characteristics including laminar position, gene expression profile and axonal targets. The cortex is generated in an inside-out fashion such that cortical projection neurons generated early in development occupy deep layers (layers 5 and 6), while those that reside in upper layers (layers 2–4) are generated later (McConnell et al., 1995; Hevner et al., 2006; Molyneaux et al., 2007).

All cortical projection neurons are generated by neural progenitors in the proliferative region of the cortex, encompassing both the ventricular and subventricular zones (VZ and SVZ) (Haubensak et al., 2004; Farkas and Huttner, 2008). To date, three different types of neural progenitors have been identified: radial glia, outer radial glia and basal progenitors. They each have distinct roles during neurogenesis and can be distinguished by characteristics including morphology, location of cell body and expression of molecular markers (Farkas and Huttner, 2008; Wang et al., 2011a; Shitamukai and Matsuzaki, 2012).

At the onset of neurogenesis, neuroepithelial cells differentiate into radial glia (Shitamukai and Matsuzaki, 2012), which can be genetically defined by their expression of transcription factors, PAX6 and SOX2 (Gotz et al., 1998; Tarabykin et al., 2001; Bani-Yaghoub et al., 2006). Highly polarized, radial glia have apical and basal processes that attach to ventricular and pial surfaces of the cortex, respectively (Shitamukai and Matsuzaki, 2012). Their cell bodies reside in the VZ and they can undergo multiple rounds of cell division, which take place at the ventricular surface (Pontious et al., 2008). Radial glia can self-renew and also divide to generate basal progenitors, outer radial glia and cortical neurons (Shitamukai et al., 2011; Shitamukai and Matsuzaki, 2012). However, the main function of radial glia is likely to expand the progenitor pool (Kowalczyk et al., 2009; Lui et al., 2011; Wang et al., 2011b).

Basal progenitors, the second major class of neural progenitors, uniquely express TBR2, a T-box transcription factor (Arnold et al., 2008; Sessa et al., 2008; Kowalczyk et al., 2009). Unlike radial glia, basal progenitors are multipolar, lack apico-basal processes and their cell bodies reside throughout the SVZ. Although some have reported the potential for few rounds of self-renewing divisions, basal progenitors predominantly undergo neurogenic symmetric division (Farkas and Huttner, 2008; Noctor et al., 2008; Shitamukai and Matsuzaki, 2012). Thus, the main function of basal progenitors is the generation of cortical neurons (Noctor et al., 2004; Pontious et al., 2008; Kowalczyk et al, 2009).

Outer radial glia, the third subclass of neural progenitor, are similar to radial glia in that they have a basal process and express PAX6 and SOX2. However, they lack an apical process and their cell bodies reside in the superficial (outer) region of the SVZ (oSVZ). They are capable of asymmetric self-renewal and also generate neurons or basal progenitors (Reillo et al., 2011; Shitamukai et al., 2011; Wang et al., 2011a, 2011b; Shitamukai and Matsuzaki, 2012). Previous work showed that outer radial glia complete many rounds of self-renewal, exhibit enhanced transit amplification and generate basal progenitors, likely contributing to

neocortical expansion in human brains (Hansen et al, 2010; Lui et al., 2011; Reillo et al., 2011). However, there are significantly fewer outer radial glia in the rodent brain and their role in neurogenesis is not fully understood.

Despite well-defined characteristics unique to neural progenitor subtypes, molecular mechanisms regulating their proliferation and differentiation remain undetermined. One genetic candidate in neural progenitor cell maintenance is NFIB, a member of the Nuclear Factor One (NFI) family of transcription factors that is essential for normal brain development. Mice with an *NfiB* gene mutation ($NfiB^{-/-}$) have enlarged lateral ventricles, agenesis of the corpus callosum, defects in the formation of the hippocampus, basilar pons and midline structures and die at birth due to lung defects (Plachez et al., 2008; Kumbasar et al., 2009; Piper et al., 2009). NFIB regulates the migration and axonal projection of cerebellar granule neurons (Wang et al., 2007; Mason et al., 2009; Heng et al., 2012). Furthermore, NFIB is expressed in the proliferative zone and in subcerebral and corticothalamic projection neurons (Plachez et al., 2008; Mason et al., 2009; McKenna et al., 2011), but its role in regulating neural progenitor maintenance and development of these neurons remains to be elucidated.

In this study, we investigated the function of *NfiB* in differentiation and expansion of distinct neural progenitor subpopulations. Additionally, we characterized its role in cortical neuron development. Similar to previous studies, we found that NFIB was expressed in corticofugal neurons and the proliferative zone throughout development (Plachez et al., 2008; Mason et al., 2009; McKenna et al., 2011). Specifically, we identified high expression of NFIB in radial glia and observed defects in both neurogenesis and cortical neuron differentiation in $NfiB^{-/-}$ mice. Radial glia failed to generate outer radial glia and basal progenitors during late corticogenesis, corticothalamic and subcerebral axons were severely diminished, and late-born neurons ectopically expressed early-born neuronal marker, CTIP2, and displayed migration defects. Additionally, genes that regulate cell cycle progression, neuronal differentiation and axon projection were mis-regulated in $NfiB^{-/-}$ cortices, as revealed by gene expression analysis. Our study clearly demonstrates that NFIB is essential in regulating differentiation of radial glia, migration of cortical projection neurons and development of corticofugal axons.

## Materials and Methods

Abbreviations used are listed in Table 1.

### Generation of $NfiB^{-/-}$, $NfiB^{-/-}$;$Fezf2^{+/PLAP}$ and $NfiB^{-/-}$;Golli-τ-$GFP^{+}$ mice

The generation of the following mouse strains were described previously: $NfiB^{+/-}$ (Steele-Perkins et al., 2005), Golli-τ-$GFP^{+}$ (Jacobs et al., 2007), and $Fezf2^{+/PLAP}$ (Chen et al., 2005a). $NfiB^{+/-}$ mice were time-mated to generate $NfiB^{+/+}$ and $NfiB^{-/-}$ embryos. $NfiB^{+/-}$ and $Fezf2^{+/PLAP}$ mice were mated to generate $NfiB^{+/-}$; $Fezf2^{+/PLAP}$ mice. These mice were then time-mated with $NfiB^{+/-}$ mice to generate $NfiB^{+/+}$;$Fezf2^{+/PLAP}$, $NfiB^{+/-}$;$Fezf2^{+/PLAP}$ and $NfiB^{-/-}$;$Fezf2^{+/PLAP}$ embryos for PLAP staining studies of axonal projections. $NfiB^{+/-}$ and Golli-τ-$GFP^{+}$ mice were mated to generate $NfiB^{+/-}$;Golli-τ-$GFP^{+}$ mice. These mice were then time-mated to $NfiB^{+/-}$ to generate $NfiB^{+/+}$;Golli-τ-$GFP^{+}$ and $NfiB^{-/-}$;Golli-τ-

*GFP*$^{+}$ embryos for GFP immunostaining of axonal projections. To acquire timed-pregnant mice, male and female mice were put together overnight. The following morning, females were inspected for a vaginal plug; observation of a plug day was defined as embryonic day (E)0.5. Postnatal day (P)0 was designated as the day of birth. Genders of embryonic mice were not determined.

All embryos were genotyped by PCR. Genotyping of *NfiB* alleles was accomplished using two sets of primers. The wild type allele was genotyped by using p1 (GCTGAGTTGGGAGATTGTGTC) and p2 (TTCTGCTTGATTTTCGGGCTTC) with an expected PCR product of about 300bp. The PCR conditions were 94°C for 2 min, followed by 30 cycles of 94°C for 30 sec, 64°C for 1 min and 72°C for 1 min. The mutant allele was genotyped using primers, p3 (TTTCCATGTTGCCACTCGC) and p4 (AACGGCTTGCCGTTCAGCA). This set of primers detects the LacZ gene, yielding a product of about 400bp. The PCR conditions were 94°C for 2 min, followed by 30 cycles of 94°C for 30 sec, 55°C for 1 min and 72°C for 1 min. Genotyping of *Fezf2* alleles was previously reported (Chen et al., 2005a). To determine whether embryos contained a copy of a *Golli-τ-GFP* allele, we used one set of primers, p5 (CCTACGGCGTGCCAGTGCTTCAGC) and p6 (CGGCGAGCTGCACGCTGCGTCCTC), yielding an expected product of about 300bp. PCR conditions were 94°C for 5 min, followed by 30 cycles of 94°C for 20 sec, 55°C for 30 sec and 72°C for 1 min. All experiments and animal husbandry were executed in accordance with protocols approved by the Institutional Animal Care and Use Committee at University of California, Santa Cruz and institutional and federal guidelines.

## Antibody characterization

Antibodies, sources and dilutions that they were used at are listed in Table 2.

**β-Gal—**The anti-βGal antibody detects the full length native β Galactosidase, a protein encoded by the *lacZ* gene in the lac operon of *E. coli*. In the *NfiB* mutant allele, the *lacZ* gene and a nuclear localization sequence were inserted into the *NfiB* locus resulting in the expression of β-Galactosidase within cells expressing the *NfiB* mutant allele (Plachez et al. 2008). Using an *NfiB*$^{+/-}$ brain, we use the anti-βGal antibody to show that β-Galactosidase expression recapitulates that of NFIB protein (Figure 1).

**BETA3 (officially BHLHE22; also known as BHLHB5)—**The anti-BETA3 antibody specifically detects a single band at 55 kDa on western blots of rat lung and brain extracts (manufacturer's information). We used the anti-BETA3 antibody to label cortical projection neurons of layers 2–5 of the cortex. BETA3 expression in *NfiB*$^{+/+}$ mice is consistent with that of previously published results (Joshi et al., 2008).

**BrdU—**The anti-BrdU antibody specifically detects bromodeoxyuridine (BrdU), a haplopyrimidine that labels proliferating cells in S phase (Struikmans et al., 1997). This was confirmed by testing the antibody's precipitation against 5-Methyl Cysteine (5-MeC), BrdU or no antigen (as a control). There was an 8-fold increase of reactivity with BrdU over 5-MeC (manufacturer's information). We, and others, have shown that use of this anti-BrdU

antibody allows for analysis of neurogenesis (Taupin 2007; McKenna et al., 2011). In this study, we inject BrdU into mice and then use the anti-BrdU antibody to identify neural progenitors in S-phase and, based on signal intensity, neurons born on the day of BrdU injection (see Material and Methods for BrdU incorporation analysis). Note: antigen retrieval is needed for this antibody (10mM Citrate Buffer in PBS; 10 min at 95°C).

**Cleaved Caspase-3 (officially CASP3; also known as CC3, CPP32 and SCA-1)—**The anti-Cleaved Caspase-3 (Asp175), or anti-CC3, antibody specifically detects bands at 17 or 19 kDa on western blots of HeLa, NIH/3T3 and C6 cell extracts representing the large fragment of activated caspase-3 resulting from cleavage of this protein adjacent to Asp175 (manufacturer's information). Immunostaining with this antibody detects apoptotic cell death *in vitro* and on brain tissue. Staining was evident in HT-29 cells treated with cell-death-inducing Staurosporine (Cell Signaling #9953), but not in untreated cells (manufacturer's results). In newborn rat brain tissue, the antibody detected apoptotic cells in transient cerebral ischemic tissue versus control (Dr. Bingren Hu, University of Miami School of Medicine, Florida) and in the vomeronasal organ of *Fezf2*$^{-/-}$ mice (Eckler et al., 2011). In this study we used the anti-CC3 antibody to detect and quantify apoptotic cells within the proliferative zones in *NfiB*$^{+/+}$ and *NfiB*$^{-/-}$ mice.

**CTIP2 (officially BCL11B; also known as Rit1); clone 25B6—**The rat monoclonal anti-CTIP2 antibody (clone 25B6) specifically detects two bands at about 95–100 kDa on a western blot of Jurkat cells immunoprecipitated with anti-Sir2 antibody and mouse brain tissue lysate. Immunohistochemical specificity was confirmed by staining on mouse cortical, spinal cord and hippocampal tissue (manufacturer's information). CTIP2 is expressed in postmitotic neurons residing in layers 5 and 6 of the mouse cortex and is critical for development of corticospinal motor neurons (Chen et al., 2005a; McKenna et al., 2011). In this study we use the anti-CTIP2 antibody to detect layer 5 and 6 neurons throughout cortical development.

**DARPP32 (officially known as PPP1R1B); clone EP27Y—**The mouse monoclonal anti-DARPP32 (clone EP27Y) antibody specifically detects a band of approximately 32 kDa on western blots of rat brain lysate (manufacturer's information). DARPP32 expression is cytoplasmic and was reported in layer 6 neurons (Molyneaux et al., 2005); we also observed the same staining pattern (McKenna et al., 2011). In our study, we use the anti-DARPP32 antibody to identify layer 6 postmitotic neuronal cell bodies and processes in *NfiB*$^{+/-}$ and NfiB$^{-/-}$ brains at E18.5. We use DP32 as nomenclature for this antibody (see Table 1).

**GFP—**The anti-GFP antibody specificity was confirmed by both western blot and immunohistochemical analyses (manufacturer's information) using transgenic mice expressing the green fluorescent protein (GFP) gene product. In this study, we use the anti-GFP antibody to detect the expression of GFP protein in *NfiB*$^{+/+}$*;Golli-τ-GFP*$^{+}$, *NfiB*$^{+/-}$*;Golli-τ-GFP*$^{+}$ and *NfiB*$^{-/-}$*;Golli-τ-GFP*$^{+}$ brains. In these mice, the *Golli-τ-GFP* allele directs expression of GFP in cell bodies and axons of deep layer cortical neurons (Jacobs et al., 2007).

**Ki67; clone B56—**The mouse monoclonal Ki67 antibody (clone B56) specifically detects a double band at 345 and 395 kDa on western blots of proliferating cells. Ki67 is a nuclear cell-proliferation associated antigen expressed in all active stages of the cell cycle (manufacturer's information). Antibody specificity is validated in various ways: In flow cytometric analysis, reactivity to the Ki67 immunogen by the Ki67-B56 antibody is blocked by a second Ki67 antibody (clone MIB). Immunostaining with the antibody (clone B56) on human tonsil, successfully labels proliferating cells (manufacturer's results). In this study, we used the Ki67 antibody to label neural progenitors and perform quit fraction analyses at different stages throughout development, as we have done previously (McKenna et al., 2011). This antibody requires antigen retrieval.

**NFIA—**The anti-NFIA antibody specifically detects a single band at about 50 kDa on western blots of MCF-7, HeLa (manufacturer's information) and JEG-3 cells (Plachez et al., 2008). In an electromobility shift assay, addition of the NFIA probe and antibody results in a supershift. However, in the presence of a neutralizing peptide, there is no shift, indicating antibody specificity (manufacturer's information). Additionally, the antibody did not cross-react against other NFI proteins nor did it detect any signal in *NfiA*$^{-/-}$ mice (Plachez et al., 2008). Here, we use the anti-NFIA antibody, as others have, to label postmitotic neurons of layers 5/6 and neural progenitors in E18.5 *NfiB*$^{+/-}$ and *NfiB*$^{-/-}$ brains (Plachez et al., 2008).

**NFIB—**The anti-NFIB antibody specifically detects a band at about 50 kDa on western blots of rat liver nuclear extract. Addition of the immunizing peptide eliminates the band, thereby confirming specificity of the antibody (manufacturer's information). Immunostaining showed specificity, such that the antibody did not cross-react with other NFI proteins nor was any staining detected in *NfiB*$^{-/-}$ mice (Plachez et al., 2008). Similar to previous protocols (Palchez et al., 2008; McKenna et al., 2011), we use the anti-NFIB antibody to label layer 5/6 postmitotic neurons and neural progenitors and analyze its co-expression with other factors critical for cortical development.

**PAX6 (also known as SEY or AN2)—**The anti-PAX6 antibody specifically detects PAX6 protein expression by immunohistochemical analysis of mouse retina, brain tissue and human epididymis tissue (manufacturer's information). PAX6 expression has been reported in both radial glia and outer radial glia in the developing cortex (Davis and Reed, 1996; Gomez-Lopez et al., 2011). Here, we use the anti-PAX6 antibody to identify radial glia and outer radial glia in *NfiB*$^{+/+}$ and *NfiB*$^{-/-}$ brains throughout cortical development.

**PHH3; clone 6G3—**The mouse monoclonal anti-phosphorylated histone H3 (Ser10) antibody (clone 6G3), or anti-PHH3 antibody, recognizes endogenous histone H3 only when it is phosphorylated at serine 10, a hallmark of cells in M phase (manufacturer's information). It specifically detects a band at 16.5 kDa on western blots of NIH/3T3 whole cell lysate treated with serum plus calyculin A (which induces phosphorylation) but not on untreated lysate. Flow cytometric analysis of pacilitaxel-treated THP1 cells using this antibody revealed higher DNA content in cells stained by the antibody, corresponding to cells that progressed through S phase and into M phase of the cell cycle. Specificity was also confirmed by co-immunostaining NIH-3T3 cells with anti-PHH3 and anti-tubulin

antibodies, and by staining in mouse subventricular zone and third instar *Drosophila* larval neuroblasts. PHH3 staining is evident in prophase, metaphase and anaphase of mitosis but is absent in non-mitotic cells and in cells pre-treated with phosphatase or phosphohistone H3 (Ser10) blocking peptide (Cell Signaling, #1000) (manufacturer's results). We use the anti-PHH3 antibody to detect and quantify mitotic cells in $NfiB^{+/+}$ and $NfiB^{-/-}$ brains throughout cortical development.

**SATB2—**The anti-SATB2 antibody detects a band at approximately 85 kDa on western blots of mouse brain tissue lysate and immunofluorescent staining revealed expression in human osteosarcoma 2 cell nuclei (manufacturer's information). SATB2 is an established marker of callosal projecting neurons (Alcamo et. al, 2008; Britanova et. al, 2008; Chen et al., 2008; McKenna et al., 2011). In this study, we use the anti-SATB2 antibody in combination with deep layer markers to identify layer 2–4 neurons and define upper cortical layers in $NfiB^{+/+}$ and $NfiB^{-/-}$ mice.

**SOX2 (also referred to as ANOP3); clone Y-17—**The anti-SOX2 antibody specifically detects a band at 34 kDa on western blots of human and mouse embryonic stem cell lysates. Immunofluorescence staining is evident in the mouse embryonic stem cell nuclei (Dr. Nobuaki Kikyo, Stem Cell Institute, University of Minnesota). It was reported that SOX2 is expressed in radial glia and outer radial glia in developing mouse cortex (Wang et al., 2011a). In this study, we use the anti-SOX2 antibody to label and quantify these two cell types in $NfiB^{+/+}$ and $NfiB^{-/-}$ mice, throughout cortical development.

**TBR1 (also referred to as TES-56)—**The anti-TBR1 antibody specifically detects a band at 74 kDa on western blots of mouse and rat hippocampal whole cell lysates (manufacturer's results). Immunostaining with this antibody revealed nuclear staining in human cortical tissue (manufacturer's results), pyramidal neurons of rat brains (Ruma Raha-Chowdhury), rat cortical neurons in culture (Dr. Ioana Carcea), and layer 6 neurons of embryonic and adult mouse cortical tissue (manufacturer's results and Dr. Carlos Perez-Garcia), all which confirmed its specificity. McKenna et al., additionally showed specificity in layer 6 neurons of the developing mouse cortex. In this study, we use the anti-TBR1 antibody to identify layer 6 neurons in $NfiB^{+/+}$ and $NfiB^{-/-}$ brains at E18.5.

**TBR2 (officially EOMES)—**The anti-TBR2 antibody detects a 72 kDa band on western blots of human mesoderm lysate, mouse brain tissue lysate and EL4 cells expressing a V5 tagged Eomesodermin. However, no band was detected when using the TBR2 antibody on human mesoderm whole cell lysate incubated with TBR2 blocking peptide (Abcam, #ab25698), or on EL4 cells expressing an empty vector or V5 tagged vector, thus validating antibody specificity (manufacturer's results). Immunostaining results showed specificity to developing mouse cerebral cortical tissue (Guillermo Estivill-Torrus), human embryonic stem cells that differentiated into mesoderm (Ludovic Vallier, University of Cambridge), and in adult mouse hippocampal tissue (Hongjun Song Lab). As others have done (Arnold et al., 2008), we use the anti-TBR2 antibody to detect and analyze basal progenitors in $NfiB^{+/+}$ and $NfiB^{-/-}$ brains throughout cortical development.

**Tuj1—**The mouse Tuj1 monoclonal antibody has been used to detect the neuronal class III β-tubulin protein (officially known as TUBB3) in axons and dendrites of postmitotic neurons (Casanovas et al., 2008). It was produced from the Tuj1 hybridoma mouse clone developed from immunizing mice with rat brain microtubules. The Tuj1 antibody does not react with β-tubulin in glial cells and staining on rat hippocampal tissue revealed immunohistochemical specificity (manufacturer's results). In this study we use laminar position of Tuj1 positive cells to determine location of postmitotic neurons within the cortex on *NfiB*$^{+/+}$ and *NfIB*$^{-/-}$ mice.

## Immunohistochemistry

To obtain embryonic tissue, pregnant mice were sacrificed by cervical dislocation and embryos were removed. E12.5 heads were drop-fixed in 4% paraformaldehyde in 1x phosphate buffered saline (PBS; pH 7.4) at 4°C. E13.5–E16.5 brains were dissected from skull then drop-fixed in 4% paraformaldehyde (PFA) in 1x PBS at 4°C. Older embryos were transcardially perfused with PBS followed by 4% PFA in 1x PBS before drop-fixation as above. All embryonic brains were cryoprotected in 30% sucrose, frozen in Optimal Cutting Temperature Compound (Tissue-Tek) and cut using a cryostat or sliding microtome. Coronal or sagittal sections were cut at 20μm via cryostat (Figures 1–4, 6–11) or 50μm (Figure 5) on sliding microtome.

For immunofluorescence, sections were blocked in 5% horse serum and 0.1%Triton X-100 in 1x PBS for 1 hour at room temperature. Sections were incubated with primary antibodies at appropriate dilutions (Table 2) overnight at 4°C. The following day, slides were washed with 0.1%Triton X-100 in 1x PBS three times for five minutes, incubated with Alexa Fluor-conjugated secondary antibodies for one hour at room temperature, then washed with 1x PBS for three times at 5 minutes before mounting with Fluoromount (Southern Biotech). Secondary antibodies used in this study were Donkey Anti-Mouse IgG Alexa Fluor 547 or 647, Donkey Anti-Rabbit IgG Alexa Fluor Cy3, Cy5 or 488, Donkey Anti-Sheep IgG Alexa Fluor 488 or 647, Donkey Anti-Chicken IgG Alexa Fluor Cy3 or 488, Donkey Anti-Rat IgG Alexa Fluor 488 or 647 and Donkey Anti-Goat IgG Alexa Fluor Cy3, 488 or 647 (all at 1:1000; Jackson ImmunoResearch Laboratories, West Grove, PA).

Nuclei were visualized using DAPI (4′,6-Diamidino-2 Phenylindole; at 1:10,000; Molecular Probes) (Figure 9) or DRAQ5 (1,5-bis((2-(dimethylamino) ethyl)amino)-4, 8-dihydroxyanthracene-9, 10-dione; at 1:5000; Cell Signaling Technology) (Figure 6). At least 3 brains/genotype were analyzed for all experiments; all tissue sections were collected onto Superfrost slides (Fisher Scientific).

## Detection of PLAP activity

Human placental alkaline phosphotase (PLAP) staining (Figure 5A–H) was performed as previously described (Chen et al., 2005a). Brain tissue was collected and sectioned at 50μm using a sliding microtome, washed in 1x PBS and post-fixed in 4% PFA in 1x PBS at 4°C for 1 hour. Sections were again washed with 1x PBS, then incubated at 70°C for 1 hour in 1x PBS. Sections were incubated with NBT/BCIP (1 mg/ml nitroblue tetrazolium/0.1 mg/ml

5-bromo-4-chloro-3-indolyl phosphate in 100 mM Tris·Hcl, pH 9.5/100 mM NaCl) at 37°C for 3 hours, then washed with 0.3% Triton X-100 in 1x PBS and mounted in Fluoromount.

### *In situ* hybridization

Non-radioactive *in situ* hybridization was essentially performed as previously described (Schaeren-Wiemers and Gerfin-Moser, 1993). Slides with fixed brain sections were post-fixed in 4% PFA for 10 minutes, treated with proteinase K for 10 minutes, fixed again in 4%PFA for 10 minutes and acetylated for 10 minutes, all at room temperature, with DEPC PBS washes in between each step. Slides were prehybridized for 2 hours at 65°C, hybridized with Digoxigenin (DIG) labeled cRNA and sealed with coverslips (HybriSlip, Grace Bio-Labs). The cDNA templates for cRNA probes for *Notch1*, *Hes1* and *Hes5* genes were generous gifts from Drs. Toshiyuki Ohtsuka and Ryoichiro Kageyama from Kyoto University, Kyoto, Japan. Nucleotides 4270–5611 of mouse *Notch1* cDNA was used to prepare the *Notch1* probe. Full-length cDNA sequences for *Hes1* and *Hes5* were used to prepare *Hes1* and *Hes5* probes, respectively. Slides were then placed in a humidity chamber overnight at 65°C. The following day, slides were washed with SSC, incubated with RNase A at 37°C for 30 minutes and washed with the following: SSC, 0.1MTris (pH 7.4)/0.15M NaCl (Buffer 1) for 5 minutes, Buffer 1 containing 1% heat inactivated goat serum for one hour at room temperature. Slides were incubated with an anti-DIG antibody in a humidity chamber overnight at 4°C. On the third day, slides were washed with Buffer 1 and equilibrated with 0.1M Tris (pH9.5)/0.1M NaCl/50mM $MgCl_2$ (Buffer 2) for 5 minutes at room temperature. To visualize probe-tissue interaction, slides were incubated for 6 hours with NBT/BCIP substrate in Buffer 2. Slides were washed with PBS, then with PBS containing 0.3% Triton X-100. Lastly, slides were fixed with 4% PFA and mounted with Fluormount-G.

### Image acquisition and digital retouching

Images for quantitative analyses were captured on a Leica SP5 confocal microscope. The detector gain was set such that <1% of pixels were saturated. Additional fluorescent and bright field images were captured on an Olympus BX51 microscope and Q-imaging Retiga camera. Adjustments of contrast and brightness and image cropping for presentation were done using Adobe Photoshop to the same degree on entire images of $NfiB^{+/+}$ and $NfiB^{-/-}$ matched cortical sections.

### Quantitative analyses

For all measurements and cell-counting, statistical analyses were performed by an unpaired t-test; significance was defined as $*p \leq 0.05$, $**p \leq 0.005$, $***p \leq 0.0005$; error bars represent standard error of means (SEM). Specific numbers of mice used in each quantitative experiment can be found in figure legends. Briefly, at least nine matched sections/age from anterior, middle and posterior regions from at least three mice/genotype were used in each quantitative comparison. Matched sections were defined as brain sections from approximately the same anterior-posterior axial position in $NfiB^{+/+}$ and $NfiB^{-/-}$ littermates. Unless otherwise noted, data presented in figures are from sections midway along the anterior-posterior axis of the brain.

**Measurements of cortical area thickness—**To measure independent thicknesses of upper layers (UL-S) or deep layers (DL-C), coronal sections of *NfiB*$^{+/+}$ and *NfiB*$^{-/-}$ mice were immunostained as described above with antibodies against SATB2 and CTIP2. DL-C was defined as the region along the dorsal-ventral (D–V) axis containing CTIP2-expressing cells; UL-S was defined as the region containing SATB2-expressing cells dorsal to DL-C, along the D–V axis (schematic Figure 4Q). For each cortical image, three measurements were taken along 300μm of the mediolateral axis and averaged. To measure the proliferative zone, the region containing the VZ, SVZ and oSVZ (VZ + o/SVZ), *NfiB*$^{+/+}$ and *NfiB*$^{-/-}$ mice were immunostained as described above with antibodies against Ki67 and TBR2. The VZ + o/SVZ was defined as the region along the D–V axis of cells expressing Ki67 and/or TBR2 (schematic Figure 6C).

**Cell-counting analysis—**Cell counting was performed on individual Z-slices from confocal microscopic images. For each brain analyzed, the cortex was divided into anterior, middle and posterior regions. Cells on 300μm wide sections of the mediolateral axis of cortical sections expressing indicated markers were counted.

**BrdU incorporation analysis—**For analysis of cells in S-phase, BrdU (Bromodeoxyuridine at 100μg/g body weight; US biologicals, Swampscott, MA) was intraperitoneally (i.p.) injected into timed pregnant mice at E18.5; embryos were collected 2 hours post-injection and processed for BrdU immunostaining and quantification. To analyze the distribution of BrdU-labeled cells, cortices were divided into ten bins of equal thickness and BrdU-labeled cells in each bin were quantified (schematic Figure 6N). For birthdating analysis, BrdU (100 μg/g body weight) was i.p. injected into timed pregnant mice at E15.5; embryos were collected at E18.5 and processed for BrdU immunostaining and quantification. Only strong BrdU-labeled cells, cells with ≥75% BrdU nuclei saturation, were counted. The distribution of strong BrdU-labeled cells was analyzed by binning, as described above.

**Quit fraction analysis—**BrdU (100 μg/g body weight) was i.p. injected into timed pregnant mice at E11.5, E12.5, E13.5, E14.5 or E15.5. Embryos were collected 24 hours later and processed for BrdU and Ki67 immunostaining, as described above. The numbers of all cells stained for BrdU (all BrdU$^{+}$) and cells stained for BrdU but not for Ki67 (BrdU$^{+}$Ki67$^{-}$) were counted. The quit fraction (QF%) was calculated as the percentage of BrdU$^{+}$Ki67$^{-}$ among all BrdU$^{+}$ cells.

## RNA sequencing (RNA-seq) and data analysis

E15.5 *NfiB*$^{+/+}$ and *NfiB*$^{-/-}$ cortices were dissected (n=3/genotype), total RNAs were isolated from each cortex (Qiagen RNAeasy kit) and used to prepare RNA-seq libraries (Illumina RNA Truseq Library Prep protocol). Libraries were paired-end (50 nucleotides per end) sequenced on Illumina Hiseq2000 platform. Between 77 and 88 million read pairs were obtained for each sample. After filtering out read pairs that matched elements in the mouse RepeatMasker library (Smit et al, 1996–2010) (less than 2% per sample), reads were mapped to the UCSC (mm9) mouse assembly with TopHat (Trapnell et al., 2009), using Bowtie (Langmead et al., 2009) as the underlying aligner. Only uniquely-mapping, fully-

paired reads were kept and potential PCR duplicates were removed using SamTools (Li et al., 2009). Between 49 and 57 million mapped read pairs remained per sample. From these mappings, the count of reads was determined for the canonical transcript of each gene in the set of UCSC Known Genes (Hsu et al., 2006) for the UCSC mm9 mouse assembly. These counts were analyzed for differential expression of genes between $NfiB^{+/+}$ and $NfiB^{-/-}$ samples using DESeq (Anders and Hubers, 2010), which models the expression variation within replicates as a function of total gene expression, to determine the significance of expression differences between conditions. A threshold for significance was set at the DESeq adjusted p-value of 0.1.

To understand the biological meaning of the output gene list, we used the Database for Annotation, Visualization and Integrated Discovery (DAVID) (Huang et al., 2009a, 2009b). The list of differentially expressed genes was uploaded into DAVID then analyzed by functional annotation clusters. A summary of gene clusters exhibiting the highest enrichment scores are in Table 3 and 4.

## Results

### NFIB is expressed in radial glia and corticofugal neurons throughout corticogenesis

NFIB is expressed in both deep layer neurons and neural progenitor cells (Mason et al., 2009; McKenna et al., 2011), but its expression profile in individual subtypes of neural progenitors is not known. To determine which progenitor cells expressed NFIB during cortical development, we used specific antibodies on E12.5–E18.5 brain sections to co-label cells expressing NFIB against known neural progenitor and layer-specific neuronal markers. Taking advantage of the *LacZ* insertion into the *NfiB* locus of $NfiB^{+/-}$ mice (Steele-Perkins et al., 2005), in addition to $NfiB^{+/+}$ mice, we used $NfiB^{+/-}$ mice to maximize detection of NFIB and cell-type specific marker co-expression. To ensure βGAL was an appropriate marker of NFIB-expressing cells, we performed immunohistochemistry with antibodies against βGAL and NFIB and found that βGAL expression recapitulates that of NFIB in $NfiB^{+/-}$ brains (Figure 1).

Immunohistochemical analysis of E12.5 and E13.5 brains revealed coexpression of NFIB and Ki67, confirming NFIB expression in neural progenitors (Figure 2A, E, P and T) (Plachez et al., 2008; Mason et al., 2009). Starting at E12.5, two major progenitor cell types were present: radial glia and basal progenitors. Radial glia in the ventricular zone (VZ) were $SOX2^{+}PAX6^{+}$ (Figure 2F–H and J). Basal progenitors in the SVZ were $TBR2^{+}SOX2^{low}$ (Figure 2K–M and O) (Arnold et al., 2008). βGAL was expressed at high levels in all $SOX2^{+}PAX6^{+}$ radial glia (Figure 2F–J), but expression was generally low or completely absent in $TBR2^{+}$ basal progenitors, despite the presence of a few $TBR2^{+}\beta GAL^{+}$ cells (Figure 2K–O). It is likely that these $TBR2^{+}\beta GAL^{+}$ cells were in transition from radial glia to basal progenitors, or from basal progenitors to neurons. Similarly, very few $TBR2^{+}$ basal progenitors expressed βGAL at E15.5 or E18.5 (Figure 2EE, 2II and 3E).

Beginning at E15.5, the presence of outer radial glia, identified by SOX2 expression in the outer subventricular zone (oSVZ), became apparent (Figure 2W, and FF). Both $SOX2^{+}$ and $PAX6^{+}$ radial glia expressed NFIB (or βGAL) at E15.5 and E18.5, however, only low-level

expression was apparent in outer radial glia (Figure 2U, Y, Z, DD, EE, FF, II and 3A, C). Together, these data demonstrate that during corticogenesis, radial glia express NFIB, but expression is almost entirely excluded from basal progenitors and outer radial glia.

We next characterized NFIB expression in the developing cortical plate. Immunostaining analyses revealed co-expression of NFIB and known markers of corticofugal projection neurons. Subcerebral marker, CTIP2, and NFIB were co-expressed in deep layers of the cortical plate at E12.5 and E13.5 (Figure 2A, E, P and T), the time when these neurons are generated (Leone et al., 2008; McKenna et al., 2011). $CTIP2^+$ neurons also expressed NFIB (or βGAL) at E15.5 (Figure 2U, Y, Z, DD).

To further characterize the molecular identity of NFIB-expressing cells, we analyzed co-expression with NFIA, DARPP32 and SATB2 (Figure 3G, I, K). NFIA, another transcription factor in the *Nfi* gene family, is expressed in proliferative zones and deep layer cortical neurons (Plachez et al., 2008; Mason et al., 2009), but whether NFIA and NFIB are expressed in the same cells is unknown. We observed βGAL and NFIA co-expression in the VZ and layer 6 (Figure 3G). βGAL was also co-expressed with layer 6 corticothalamic marker, DARPP32 (Molyneaux et al., 2005) (Figure 3I). Conversely, there was little co-expression with SATB2, a known marker of callosal projection neurons (Alcamo et. al, 2008; Britanova et. al, 2008; Chen et al., 2008) (Figure 3K). However, of the few $SATB2^+\beta GAL^+$ neurons, most were located in layer 6 (Figure 3K). Additionally, NFIB and βGAL expression was noticeably stronger in postmitotic neurons compared to that in neural progenitors (Figure 2). Collectively, analysis of neuronal marker expression indicates that NFIB is expressed in corticofugal neurons throughout corticogenesis and may also be expressed in a small subset of deep layer callosal projection neurons. Overall, the expression profile of NFIB throughout cortical development suggests it may regulate neurogenesis and differentiation of radial glia and corticofugal neurons.

### *NfiB*$^{-/-}$ mice display a reduction in upper cortical layer thickness during late neurogenesis

To determine the function of NFIB in cortical development, we investigated what effects the loss of NFIB had on overall cortical organization in *NfiB*$^{-/-}$ mice. We first determined the molecular identity of $\beta GAL^+$ cells in E18.5 *NfiB*$^{-/-}$ mice by immunostaining with antibodies against βGAL and markers of neural progenitors or postmitotic neurons. Similar to *NfIB*$^{+/+}$ and *NFiB*$^{+/-}$ brains, we found that in *NfiB*$^{-/-}$ mice, βGAL was expressed in $SOX2^+$ and $PAX6^+$ radial glia, but expression was weak or absent in $SOX2^+$ outer radial glia and $TBR2^+$ basal progenitors (Figure 3A–F). We observed βGAL and NFIA co-expression in layer 6 and the proliferative zone (Figure 3H), and βGAL expression in $DARPP32^+$ corticothalamic projection neurons (Figure 3J). The majority of $SATB2^+$ callosal projection neurons did not express βGAL (Figure 3L) and those that did were predominantly in layer 6, similar to *NfiB*$^{+/-}$ cortices (Figure 3K–L). Together, these results indicated that the molecular identity of $\beta GAL^+$ NFIB-mutant cells was similar to NFB-expressing cells in *NfiB*$^{+/+}$ and *NfiB*$^{+/-}$ cortices.

While the overall expression of cell-type specific markers was comparable in control (*NfiB*$^{+/+}$ or *NfiB*$^{+/-}$) and *NfiB*$^{-/-}$ cortices, thickness of upper layers 2–4 appeared smaller in *NfiB*$^{-/-}$ cortices (Figure 3). To further investigate this, we compared laminar organization of

control (*NfiB*$^{+/+}$) and *NfiB*$^{-/-}$ cortices. CTIP2 expression was higher in layer 5 than in layer 6 in both control (Figure 4A, C, D) and mutant (Figure 4E, G, H) littermates. Co-immunostaining with CTIP2 and SATB2 clearly revealed a reduction in upper layer (2–4) thickness as well as a modest expansion of deep layers 5–6 (Figures 4A–H). Immunostaining with additional antibodies against layer specific markers, BETA3 and TBR1, revealed a similar outcome. In control mice, BETA3 is strongly expressed in layer 5 and to a lesser extent in upper layers (Figure 4I, K, L). However, in *NfiB*$^{-/-}$ cortices, we observed an increase in BETA3$^{+}$ cell density within layer 5 (Figure 4M, O, P), ectopic BETA3$^{+}$ neurons in layer 6 (arrows, Figure 4P) and a reduction in upper layer thickness (Figures 4I, K, L, M, O, and P). In *NfiB*$^{+/+}$ mice, TBR1 was predominantly expressed in layer 6 corticothalamic neurons, while some TBR1$^{+}$ neurons were also observed in upper layers (Figure 4J–L). However, *NfiB*$^{-/-}$ mice displayed an absence of TBR1$^{+}$ cells in upper layers (Figure 4N–P).

To quantitatively assess the loss of *NfiB* on cortical lamination, we measured and compared thicknesses of regions containing upper layer SATB2$^{+}$ neurons (UL-S) or deep layer CTIP2$^{+}$ neurons (DL-C) in *NfiB*$^{+/+}$ and *NfiB*$^{-/-}$ brains. Subsequently, this enabled comparison of overall cortical plate thickness. For measurements, we performed immunostaining with antibodies against CTIP2 and SATB2 at E16.5 and E18.5. We defined (UL-S), layers 2–4, as the cortical region containing SATB2$^{+}$ but not CTIP2$^{+}$ neurons. DL-C, layers 5 and 6, were defined as the region containing CTIP2$^{+}$ cells, regardless of SATB2 expression. Cortical plate thickness was defined as the sum of upper and deep layer thicknesses (schematic in Figure 4Q). At E16.5, the overall thickness of the cortical plate was significantly reduced in *NfiB*$^{-/-}$ mice (171.8 ± 10.9μm) compared to *NfiB*$^{+/+}$ (215.5 ± 15.1μm, $p=0.0313$), predominantly due to a reduction in UL-S thickness. In *NfiB*$^{+/+}$ mice, UL-S (41.8 ± 3.1μm) comprised approximately 19.5% of the cortical plate but in *NfiB*$^{-/-}$ littermates, UL-S (13.5 ± 2.7μm, $p<0.0001$) was only 7.7% of the cortical plate.

Likewise, at E18.5, UL-S was significantly thinner in *NfiB*$^{-/-}$ brains compared to *NfiB*$^{+/+}$ mice (*NfiB*$^{+/+}$ 90.6 ± 4.1μm vs. *NfiB*$^{-/-}$ 57.2 ± 1.6μm, $p=<0.0001$). Regardless of an overall reduction in cortex thickness (from apical to basal surfaces) (Figure 3, 4), the thickness of the cortical plate was comparable between mutant and control littermates, a result explained by an expansion of the DL-C (Figure R). Collectively, immunostaining and quantitative analysis reveal that in *NfiB*$^{-/-}$ mice, the ratio of deep to upper layers in the cortical plate shifted more toward a deep layer profile. Observed changes in cortical layer thickness in *NfiB*$^{-/-}$ mice and NFIB expression in radial glia and corticofugal neurons, together suggest that NFIB is required for proper neurogenesis and neuronal differentiation.

## *NfiB*$^{-/-}$ mice display a significant loss of corticothalamic and corticospinal axonal projections

Considering that NFIB is robustly expressed in corticofugal neurons, we asked whether NFIB is required for proper differentiation of corticofugal neurons, specifically, for axon development. To answer this, we used transgenic methods to label and analyze axonal projections. *Fezf2* (also known as *Fezl*, *Zfp312* and *Znf312*) is expressed in both subcerebral and corticothalamic projection neurons (Chen et al., 2005a; Chen et al., 2008; Leone et al.,

2008; McKenna et al., 2011). In the *Fezf2* mouse, an *ires-PLAP* (internal ribosomal entry site-Placental Alkaline Phosphatase) was inserted into the *Fezf2* open reading frame (Chen et al., 2005a), thus cell bodies and axons of subcerebral and corticothalamic projection neurons are made visible by PLAP staining. Similarly, the *Golli-τ-GFP*$^{+}$ allele directs expression of GFP in corticofugal projection neurons (Jacobs et al., 2007), allowing direct observation of GFP-labeled axons.

We analyzed corticofugal axons in *NfiB*$^{+/+}$*;Fezf2*$^{PLAP/+}$, *NfiB*$^{+/-}$*;Fezf2*$^{PLAP/+}$ and *NfiB*$^{-/-}$*;Fezf2*$^{PLAP/+}$ mice at E18.5 by PLAP staining. As expected, in *NfiB*$^{+/+}$*; Fezf2*$^{PLAP/+}$ mice, bundles of PLAP$^{+}$ axons were observed projecting through the internal capsule (Figure 5B, asterisk), toward the thalamus (Figure 5B, arrowhead) and projecting through the cerebral peduncle toward the spinal cord (Figure 5A, C, D, arrows,). There was a modest reduction of PLAP$^{+}$ corticofugal axons in *NfiB*$^{+/-}$*;Fezf2*$^{PLAP/+}$ mice (data not shown). Strikingly, in *NfiB*$^{-/-}$*; Fezf2*$^{PLAP/+}$ mice, very few PLAP$^{+}$ axons projected through the internal capsule (Figure 5F, asterisk), and axons projecting toward the thalamus (Figure 5F, arrowhead) or through the cerebral peduncle (Figure 5E, G, H, arrows) were not detected. In addition, no ectopic axons were observed. These results suggest that in the absence of *NfiB*, corticofugal neurons failed to project axons out of the cerebral cortex.

We also analyzed GFP-labeled corticofugal axons in *NfiB*$^{+/+}$*; Golli-τ-GFP*$^{+}$, *NfiB*$^{+/-}$*; Golli-τ-GFP*$^{+}$ and *NfiB Golli-τ-GFP*$^{+}$ mice at E18.5. In *NfiB*$^{+/+}$*; Golli-τ-GFP*$^{+}$ animals, GFP$^{+}$ axons projected through the internal capsule (Figure 5K, L, asterisks) toward the thalamus (Figure 5K–M, open arrows), pons (Figure 5I and J, white arrows) and cerebral peduncle (Figure 5N, white arrowheads). There was an intermediate loss of GFP$^{+}$ corticofugal axons in *NfiB*$^{+/-}$*; Golli-τ-GFP*$^{+}$ mice (data not shown). However, in *NfiB*$^{-/-}$*; Golli-τ-GFP*$^{+}$ mice, very few GFP$^{+}$ axons were detected in the internal capsule (Figure 5Q, R, asterisks) and thalamus (Figure 5Q–S, open arrows). A drastic reduction of GFP$^{+}$ axons projecting through the pons (Figure 5O and P, white arrows) and cerebral peduncle (Figure 5T, white arrowheads) was also observed. Collectively, these results showed that in *NfiB*$^{-/-}$ mice, corticofugal neurons failed to project axons to expected targets, indicating that NFIB is required for proper differentiation of corticofugal neurons.

## Loss of M phase and S phase neural progenitors within the SVZ and oSVZ during late corticogenesis

To determine the function of NFIB in neural progenitors, we first compared proliferative zone organization of *NfiB*$^{+/+}$ and *NfiB*$^{-/-}$ mice from E12.5 to E18.5 by analyzing the expression of TBR2 and Ki67. Together, these markers labeled the VZ, SVZ and oSVZ, thus defining the boundaries of the proliferative zone (VZ + o/SVZ) (Figure 6A–C). At E12.5 and E14.5, the thickness of the proliferative zone, as both an absolute measurement and as a percentage of overall cortical thickness, was similar in control and mutant mice (Figure 6D). At E16.5, *NfiB*$^{-/-}$ brains displayed a significant decrease in proliferative zone thickness compared to *NfiB*$^{+/+}$ brains (Figure 6D). As a percentage of overall cortical thickness, the proliferative zone in *NfiB*$^{+/+}$ animals made up 47.6% ± 2.2% of the cortex, while in *NfiB*$^{-/-}$, it was only 39.0% ± 5.1%, $p=0.0004$. Most notable was the striking absence of TBR2$^{+}$ cells in the oSVZ and compaction of these cells near the ventricular

surface in *NfiB*$^{-/-}$ cortices (Figure 6A–B). A significant decrease was also observed at E18.5 (*NfiB*$^{+/+}$ 41.6% ± 3.4% versus *NfiB*$^{-/-}$ 32.0% ± 3.6%, *p<0.0001*) (Figure 6D), indicating that proliferative zone thickness was specifically affected at later stages of cortical development.

To further examine defects in the proliferative zone, we analyzed neural progenitors during different phases of the cell cycle. First, we compared the number and cortical location of cells in E12.5–E18.5 *NfiB*$^{+/+}$ and *NfiB*$^{-/-}$ mice that expressed phosphorylated histone H3 (PHH3), a marker for cells in M phase (Figure 6E–I). At E12.5 and E14.5, the number of PHH3$^{+}$ cells and their cortical position were similar in *NfiB*$^{+/+}$ and *NfiB*$^{-/-}$ brains (Figure 6I). However, a significant loss of total number of PHH3$^{+}$ cells (*NfiB*$^{+/+}$ 77.1 ± 6.6 cells/mm vs. *NfiB*$^{-/-}$ 41.1 ± 3.0 cells/mm, *p=<0.0001*) was observed in E16.5 mutant brains (Figure 6E–I). The loss was due to significantly fewer PHH3$^{+}$ cells in both the o/SVZ (*NfiB*$^{+/+}$ 37.1 ± 4.0 cells/mm vs. *NfiB*$^{-/-}$ 16.1 ± 2.8 cells/mm, *p=0.0006*) and VZ (*NfiB*$^{+/+}$ 40.2 ± 3.9 cells/mm vs. *NfiB*$^{-/-}$ 25.1 ± 2.3 cells/mm, *p=0.0044*) (Figure 6E–I). Interestingly, despite a significant loss of total number of PHH3$^{+}$ cells in E18.5 *NfiB*$^{-/-}$ brains (*NfiB*$^{+/+}$ 24.1 ± 2.5 cells/mm versus *NfiB*$^{-/-}$ 16.4 ± 1.9 cells/mm, *p=0.0263*), a comparable number of PHH3$^{+}$ cells were observed in the VZ, indicating that the loss was specifically due to significantly fewer PHH3$^{+}$ cells within the o/SVZ (Figure 6I). These results suggest a loss of actively dividing neural progenitors in *NfiB*$^{-/-}$ mice during late corticogenesis, an effect more striking in the SVZ and oSVZ.

Next, we compared number and cortical distribution of neural progenitors in S phase (Figure 6J–O). BrdU was administered to pregnant mice carrying E18.5 embryos; brains were collected 2 hours later and processed for BrdU immunohistochemistry. BrdU$^{+}$ cells were quantified by cortical binning (10 bins). When individual cortices were divided into bins, there was a trend such that the marginal zone was in bin 1, the cortical plate was in bins 2–6, the SVZ and oSVZ (o/SVZ) was in bins 7–9 and the VZ was predominantly in bin 10 (Figure 6N, schematic). We determined the distribution of S phase progenitors by quantification of BrdU$^{+}$ cells in each of the following regions: the cortical plate (including the marginal zone), o/SVZ, and VZ. There was a significant loss of total number of BrdU$^{+}$ cells in *NfiB*$^{-/-}$ mice (54.6 ± 2.2 cells/100 μm, *p=0.0316*) compared to littermate controls (70.5 ± 6.5 cells/100 μm) (Figure 6J–O). While the number of BrdU$^{+}$ cells in bin 10 was similar in *NfiB*$^{+/+}$ and *NfiB*$^{-/-}$ animals, loss of total number was due to significantly fewer BrdU$^{+}$ cells in bins 7–9 (*NfiB*$^{+/+}$ 33.3 ± 2.8 cells/100 μm vs. *NfiB*$^{-/-}$ 18.5 ± 1.7 cells/100 μm, *p<0.0001*) and 1–6 (*NfiB*$^{+/+}$ 8.9 ± 1.2 cells/100 μm vs. *NfiB*$^{-/-}$ 2.0 ± 0.4 cells/100 μm, *p<0.0001*) (Figure 6O), clearly indicating a severe loss of S phase progenitors within the SVZ and oSVZ in *NfiB*$^{-/-}$ mice. Taken together with the observed reduction in proliferative zone thickness in *NfiB*$^{-/-}$ mice, these results suggest that NFIB is required for the generation or survival of neural progenitors located specifically within the SVZ and oSVZ, but not VZ.

## Outer radial glia and basal progenitors are absent in *NfiB*$^{-/-}$ mice during late corticogenesis

To determine which subclasses of neural progenitors were affected by loss of *NfiB*, we immunostained E12.5–E18.5 *NfiB*$^{+/+}$ and *NfiB*$^{-/-}$ brains with PAX6, SOX2 and TBR2 antibodies. Tuj1 (Figure 7A–L) or CTIP2 (Figure 7M–V) antibodies were used to label cortical neurons. PAX6 and Tuj1 expression was similar in *NfiB*$^{+/+}$ and *NfiB*$^{-/-}$ mice at E12.5 (Figure 7A–F). At E14.5, expression of PAX6 was unaffected in *NfiB*$^{-/-}$ mice compared to controls, as was the expression of SOX2 and TBR2 (Figure 7G, I, J, L and 8A, B, D, E, F, H). However, Tuj1 staining revealed fewer axons at E14.5, a time when most cortical neurons are of corticofugal identity (Figure 7H, I, K, L and Figure 8C, D, G, H). These results indicate that axon defects in corticofugal neurons due to a loss of NFIB begin around mid-corticogenesis (E14.5), yet all subclasses of neural progenitors were unaffected up to this timepoint.

Defects in the expression of markers for neural progenitor subtypes in *NfiB*$^{-/-}$ mice were observed during late (E16.5–E18.5) corticogenesis. In E16.5 *NfiB*$^{-/-}$ cortices, despite a similar total number, there was significantly more PAX6$^{+}$ cells in the VZ (*NfiB*$^{-/-}$ 153.9 ± 9.1 cells/100μm vs. *NfiB*$^{+/+}$ 128.9 ± 7.6 cells/100μm, $p=0.0095$), yet markedly fewer in the o/SVZ (*NfiB*$^{-/-}$ 12.9 ± 1.0 cells/100μm vs. *NfiB*$^{+/+}$ 40.4 ± 3.1 cells/100μm, $p<0.0001$) (Figure 7M, O, Q, R, T, V and EE), indicating more radial glia but a loss of outer radial glia. TBR2$^{+}$ cells were present in both the SVZ and oSVZ in *NfiB*$^{+/+}$ mice (Figure 8I and J). However, the total number of TBR2$^{+}$ basal progenitors was significantly reduced in *NfiB*$^{-/-}$ littermates (*NfiB*$^{+/+}$ 156.2 ± 10.0 cells/100μm vs. *NfiB*$^{-/-}$ 99.9 ± 3.6 cells/100μm, $p<0.0001$), and although there were significantly fewer TBR2$^{+}$ basal progenitors in the deeper SVZ, more dramatic was the loss in the oSVZ (*NfiB*$^{+/+}$ 47.2 ± 4.0 cells/100 μm vs. *NfiB*$^{-/-}$ 13.0 ± 1.2 cells/100 μm, $p<0.0001$) (Figure 8I–L and Q).

At E18.5, *NfiB*$^{-/-}$ mice displayed a loss of PAX6$^{+}$/SOX2$^{+}$ outer radial glia and TBR2+ basal progenitors (Figure 7W–EE and 8M–Q). Although there was approximately the same total number of PAX6$^{+}$ cells in *NfiB*$^{+/+}$ and *NfiB*$^{-/-}$ cortices, there were significantly fewer PAX6$^{+}$ cells in the *NfiB*$^{-/-}$ o/SVZ (Figure 7W, Y, Z, AA, CC, DD and EE). Similar to analysis at E16.5, we observed a significant decrease in the number of TBR2$^{+}$ basal progenitors in both the SVZ and oSVZ (Figure 8M–Q), Taken together, these results reveal that *NfiB*$^{-/-}$ mice have more radial glia but display a striking loss of outer radial glia and basal progenitors at E16.5 and E18.5. This suggests that NFIB may regulate the differentiation of radial glia into outer radial glia and basal progenitors during late corticogenesis.

To explain the loss of these two neural progenitor subtypes, we asked whether the absence of NFIB resulted in an increase in apoptosis or a decrease of their generation. We assayed the number of apoptotic cells in *NfiB*$^{+/+}$ and *NfiB*$^{-/-}$ cortices by immunostaining with an antibody against activated caspase 3 (CC3) at E15.5, one day prior to the observed loss of neural progenitors (Figure 9). No statistical difference in CC3$^{+}$ cell number was observed (Figure 9J), indicating that loss of outer radial glia and basal progenitors in *NfiB*$^{-/-}$ cortices was not due to cell death, but instead, due to the lack of their generation. Furthermore,

compared to the SVZ, the more severe loss of TBR2$^+$, SOX2$^+$ and PAX6$^+$ cells in the oSVZ strongly suggests that the fewer number of outer radial glia contributes to the reduction of basal progenitor generation in *NfiB*$^{-/-}$ mice.

### Late-born neurons express deep-layer neuronal marker, CTIP2, and migration is delayed

To further investigate the function of NFIB in regulating neural progenitor proliferation and differentiation, we compared the quit fractions in *NfiB*$^{+/+}$ and *NfiB*$^{-/-}$ cortices at several timepoints throughout neurogenesis. BrdU was administered to pregnant mice at E11.5, E12.5, E13.5, E14.5 and E15.5; embryonic brains were collected 24 hours later and immunostained with Ki67 and BrdU antibodies. The quit fraction was calculated as the percentage of BrdU$^+$Ki67$^-$ cells among all BrdU$^+$ cells, representing the fraction of cells that exited the cell cycle on a given day. Compared to *NfiB*$^{+/+}$ littermates, the quit fraction was unaffected in *NfiB*$^{-/-}$ cortices at E11.5, E12.5, E13.5 and E14.5. However, a significant increase was observed at E15.5 (*NfiB*$^{+/+}$ 64.5% ± 1.7% versus *NfiB*$^{-/-}$ 76.8% ± 1.8%, *p=0.0045*) (Figure 10A).

The increased quit fraction in E15.5 *NfiB*$^{-/-}$ brains suggested more neurons were generated at this time. To test this, we performed birthdating analysis by injecting BrdU into pregnant mice carrying E15.5 embryos, collecting brains at E18.5 and immunostaining with antibodies against BrdU, CTIP2, and SATB2 (Figure 10B–I). The number of E15.5 BrdU$^+$ cells (see Material and Methods) was compared between *NfiB*$^{+/+}$ and *NfiB*$^{-/-}$ cortices. Consistent with results from quit fraction analyses (Figure 10A), the number of E15.5 BrdU$^+$ cells was significantly higher in *NfiB*$^{-/-}$ brains (70.0 ± 3.1 cells/100 μm, *p=0.0001)* than controls (49.4 ± 2.8 cells/100 μm) (Figure 10B, E, F, I, J).

To address whether NFIB plays a role in migration of neurons generated at E15.5, we compared the cortical distribution of E15.5 BrdU$^+$ cells by binning (refer to schematic, Figure 6N). E15.5 BrdU$^+$ cells per bin were quantified as a percentage of total E15.5 BrdU$^+$ cells. In *NfiB*$^{+/+}$ cortices, almost all E15.5 BrdU$^+$ cells were located in the cortical plate, with many of them in upper layers (Figure 10B, E, K). Conversely, in *NfiB*$^{-/-}$ mice, a significantly higher percentage of E15.5 BrdU$^+$ cells were positioned below the cortical plate while a significantly lower percentage were in upper cortical layers (Figure 10F, I, K). This indicates a delay or improper termination of neuronal migration, which may lead to the observed thinning of upper cortical layers (Figure 3, 4 and 10E, I).

Additionally, we investigated the identity of E15.5 BrdU$^+$ cells by their expression of CTIP2 and SATB2. There was no significant difference between the percentage of E15.5 BrdU$^+$ cells expressing SATB2 in *NfiB*$^{+/+}$ and *NfiB*$^{-/-}$ cortices. However, the percentage of those expressing CTIP2 was significantly higher in *NfiB*$^{-/-}$ brains (*NfiB*$^{+/+}$ 7.9% ± 1.4% versus *NfiB*$^{-/-}$ 21.1% ± 1.9%, *p<0.0001*) (Figure 10E, I, L). Similar to BrdU staining, many more SATB2$^+$ and CTIP2$^+$ cells were located below the cortical plate in *NfiB*$^{-/-}$ cortices (Figure 10B–I), suggesting a migration defect. This possibly explains our observations of ectopic CTIP2$^+$ cells located below the cortical plate and morphological abnormalities of CTIP2$^+$ cells within the cortical plate of E16.5 *NfiB*$^{-/-}$ cortices (Figure 7N–P and S–V). In *NfiB*$^{+/+}$ mice, CTIP2$^+$ neurons in the cortical plate were round in shape, a morphology typical of neurons that have completed migration (Figure 7N–P). In *NfiB*$^{-/-}$ mice, however, CTIP2$^+$

neurons displayed an elongated morphology that is associated with neurons that are currently migrating (Figure 7S–U). Collectively, these results suggest that at E15.5, more cells exited the cell cycle and differentiated into neurons in *NfiB*$^{-/-}$ mice. They ectopically expressed early-born neuron marker, CTIP2, and their migration was defective. Thus, NFIB is required for proper neurogenesis and migration of late-born neurons.

### Genome-wide transcriptome analysis revealed that NFIB regulates axonal projection and cell cycle progression

To investigate the function of NFIB in regulating cortical neurogenesis and neuronal differentiation, we performed gene expression analysis of E15.5 *NfiB*$^{+/+}$ and *NfiB*$^{-/-}$ cortices by RNA-seq (see Material and Methods). We used the DESeq program to compare gene expression of *NfiB*$^{-/-}$ samples against controls (Anders et al., 2010) and found that expression levels of 1844 genes in E15.5 *NfiB*$^{-/-}$ mice were significantly changed. Among them, 929 were increased by at least 1.17-fold and 915 were decreased by at least 0.85-fold.

We performed gene annotation analysis using the online bioinformatics tool, DAVID (Database for Annotation, Visualization and Intergrated Discovery). Misregulated genes in *NfiB*$^{-/-}$ cortices were clustered with regards to their function; clusters were organized by enrichment score (Huang et al., 2009a; Huang et al., 2009b). Cluster 1 had the highest enrichment score and included 168 genes known to regulate cell cycle properties, such as M phase progression and cell division. There were 123 genes in Cluster 2, including transcription factors correlated with neuron differentiation and axon guidance molecules. Gene members of the Notch, Fgf, Shh and Wnt signaling pathways, all of which are important for cortical development (Gaiano et al., 2000; Cornell and Eisen, 2005; Louvi and Artavanis-Tsakonas, 2006; Dong et al., 2012; Tiberi et al., 2012), were also listed in Cluster 2. Cluster 3 included 100 genes, those of which regulate cell motion, neuron migration and cell localization (Table 3 and 4). Mis-regulation of these specific gene clusters in E15.5 *NfiB*$^{-/-}$ cortices provides further evidence that NFIB is essential for both proliferation and differentiation of cortical progenitor cells, and axonal projection of cortical neurons.

Notch signaling is essential for regulating radial glia and outer radial glia maintenance and differentiation (Cornell and Eisen, 2005; Yoon and Gaiano, 2005; Louvi and Artavanis-Tsakonas, 2006; Guillemot, 2007; Shitamukai et al., 2011; Saito, 2012). In E15.5 *NfiB*$^{-/-}$ cortices, many members of the Notch signaling pathway were mis-regulated, including Dll1, Notch3, Hes1, Hes5, Hey1, and Hey2 (Table 4 and data not shown). We performed *in situ* hybridization on E18.5 *NfiB*$^{+/+}$ and *NfiB*$^{-/-}$ brains for several of these genes (Figure 11) and found that mis-regulation of Notch1, Hes1 and Hes5 persisted throughout the remainder of cortical development. Compared to controls, expression of Notch1, Hes1 and Hes5 mRNA was significantly upregulated in the VZ (Figure 11), suggesting an increase in Notch signaling, specifically in radial glia, resulting in observed defects in radial glia differentiation in *NfiB*$^{-/-}$ mice.

## Discussion

By carefully analyzing NFIB expression at embryonic stages and investigating the defects in *NfiB*$^{-/-}$ brains, our study revealed both novel and broad functions of NFIB in regulating the

generation of cortical projection neurons, including radial glial differentiation, neuronal migration and axon projection. Multiple steps are involved in generating cortical projection neurons. First, radial glia expand the progenitor pool and generate outer radial glia, basal progenitors and neurons. Newly generated neurons migrate to their final laminar destinations, project axons and dendrites to appropriate targets to form functional neural circuits, and differentiate into mature neurons. Each of these processes is regulated by specific genetic pathways and embryonic environmental factors. A detailed comparison of $NfiB^{+/+}$ and $NfiB^{-/-}$ mice throughout cortical development revealed defects in both cortical neurogenesis and neuronal differentiation in $NfiB^{-/-}$ brains. During corticogenesis, NFIB is highly expressed in radial glia and in deep layer corticofugal neurons, suggesting important functions in regulating cortical development. Indeed, in $NfiB^{-/-}$ mice, outer radial glia and basal progenitors were absent, corticofugal neurons failed to project axons to the thalamus and spinal cord, and migration of upper layer cortical neurons was defective. Additionally, RNA-sequencing revealed a misexpression of genes regulating cell cycle, neuronal differentiation, axonal projection, and cell migration in $NfiB^{-/-}$ cortices. Together, these results demonstrated the necessity of NFIB in neural stem and progenitor cell differentiation, corticofugal axon projection, and migration of late-born cortical projection neurons. Thus NFIB regulates the development of cortical projection neurons across many levels.

Compared to radial glia and basal progenitors, despite having been discovered over three decades earlier, outer radial glia have only recently been more thoroughly investigated in mice, ferrets and humans (Hevner and Haydar, 2012). In humans, outer radial glia and basal progenitors greatly amplify the neural progenitor pool for neuronal production, which in turn, is likely responsible for the expansion of upper layer cortical neurons (Fietz et al., 2010; Hansen et al., 2010; Reillo et al., 2011; Shitamukai et al., 2011; Wang et al., 2011a, 2011b; Hevner and Haydar, 2012). Other research indicates that the basal process of outer radial glia serve as migrating scaffolds for newly born neurons in the human cerebral cortex (Reillo et al., 2011). However, in rodents, there are significantly fewer outer radial glia; their roles in cortical neurogenesis and as migration guides are not fully understood.

Our results strongly indicate the importance of outer radial glia in both generation and migration of late born cortical projection neurons in mice. Outer radial glia were absent, cortical upper layers were thinner, and late born cortical neurons exhibited a delay in migration toward the cortical plate in $NfiB^{-/-}$ mice. Among these defects, delayed migration of late-born cortical neurons may have contributed to the reduction in upper cortical layer thickness. NFIB expression in late-born neurons before birth is weak or absent (Figure 1), indicating that migration defects of these neurons in $NfiB^{-/-}$ mice may not be a direct consequence of lacking NFIB in the upper-layer neurons. The lack of a migration-scaffold provided by basal processes of outer radial glia is one likely cause of delayed migration. Additionally, ectopic expression of CTIP2 in late-born neurons in $NfiB^{-/-}$ mice suggests that lack of NFIB expression in neural progenitors can effect gene expression and differentiation of cortical neurons, which may indirectly leads to the neuronal migration defect. Collectively, these results suggest that NFIB is critical for generation of outer radial glia, and in turn, is essential for proper differentiation and migration of upper layer neurons.

To date, several genes and molecular pathways that regulate neural progenitor proliferation and differentiation have been identified. For example, increase in activation of the Notch signaling pathway in radial glia has been associated with maintaining “stemness”, while low Notch signaling is correlated with neuronal differentiation (Gaiano et al., 2000; Yoon and Gaiano, 2005; Basak and Taylor, 2007; Imayoshi et al., 2011). Here we show that several genes in the Notch signaling pathway are upregulated in *NfiB*$^{-/-}$ cortices (Table 4 and Figure 11), supporting previous results indicating that NFI family members regulate Notch signaling (Deneen et al., 2006; Mason et al., 2009; Piper et al., 2010). However, molecular mechanisms that determine the outcome of radial glial progeny are not fully understood, accordingly, further analysis of differentially expressed genes in *NfiB*$^{-/-}$ mice will provide insight into this process.

In addition to its role in generation of outer radial glia, NFIB is also essential for differentiation of corticofugal neurons as evidenced by the severe reduction of corticofugal axons in *NfiB*$^{-/-}$ mice (Figure 5). Moreover, NFIB is highly expressed in corticofugal neurons (Figures 2–4) and RNA-sequencing revealed a misexpression of genes that regulate axonal projections and axonogenesis in *NfiB*$^{-/-}$ mice (Table 3 and 4). Together, these results strongly indicate an extensive role for NFIB in differentiation of corticofugal projection neurons. Generation of a neuron-specific *NfiB* mutant mouse or selective interference of NFIB function in corticofugal neurons may further facilitate our understanding of its role in regulating corticofugal neuron differentiation and axon projection.

## Acknowledgments

We thank Drs. Richard Gronostajski at State University of New York at Buffalo for generously providing the *NfiB*$^{+/-}$ mice and Dr. Anthony T. Campagnoni from University of California, Los Angeles for providing the *Golli-τ-GFP*$^{+}$ mice. We thank Matthew Eckler, William McKenna, Chao Guo and other members of the Chen lab for technical help and scientific discussions. This work was funded by R01MH082965 from National Institute of Health (to BC), a New Faculty Award RN1-00530-1 from California Institute of Regenerative Medicine (to BC), and a training grant R25GM058903 from National Institute of Health (to JB).

## Literature Cited

Alcamo EA, Chirivella L, Dautzenberg M, Dobreva G, Farinas I, Grosschedl R, McConnell SK. Satb2 regulates callosal projection neuron identity in the developing cerebral cortex. Neuron. 2008; 57(3): 364–377. [PubMed: 18255030]

Anders S, Huber W. Differential expression analysis for sequence count data. Genome Biol. 2010; 11(10):R106. [PubMed: 20979621]

Arnold SJ, Huang GJ, Cheung AF, Era T, Nishikawa S, Bikoff EK, Molnar Z, Robertson EJ, Groszer M. The T-box transcription factor Eomes/Tbr2 regulates neurogenesis in the cortical subventricular zone. Genes Dev. 2008; 22(18):2479–2484. [PubMed: 18794345]

Bani-Yaghoub M, Tremblay RG, Lei JX, Zhang D, Zurakowski B, Sandhu JK, Smith B, Ribecco-Lutkiewicz M, Kennedy J, Walker PR, Sikorska M. Role of Sox2 in the development of the mouse neocortex. Dev Biol. 2006; 295(1):52–66. [PubMed: 16631155]

Basak O, Taylor V. Identification of self-replicating multipotent progenitors in the embryonic nervous system by high Notch activity and Hes5 expression. Eur J Neurosci. 2007; 25(4):1006–1022. [PubMed: 17331197]

Britanova O, de Juan Romero C, Cheung A, Kwan KY, Schwark M, Gyorgy A, Vogel T, Akopov S, Mitkovski M, Agoston D, Sestan N, Molnar Z, Tarabykin V. Satb2 is a postmitotic determinant for

upper-layer neuron specification in the neocortex. Neuron. 2008; 57(3):378–392. [PubMed: 18255031]

Chen B, Schaevitz LR, McConnell SK. Fezl regulates the differentiation and axon targeting of layer 5 subcortical projection neurons in cerebral cortex. Proceedings of the National Academy of Sciences of the United States of America. 2005a; 102(47):17184–17189. [PubMed: 16284245]

Chen B, Wang SS, Hattox AM, Rayburn H, Nelson SB, McConnell SK. The Fezf2, Ctip2 genetic pathway regulates the fate choice of subcortical projection neurons in the developing cerebral cortex. Proceedings of the National Academy of Sciences. 2008; 105(32):11382–11387.

Chen J-G, Rasin M-R, Kwan KY, Sestan N. Zfp312 is required for subcortical axonal projections and dendritic morphology of deep-layer pyramidal neurons of the cerebral cortex. Proceedings of the National Academy of Sciences of the United States of America. 2005b; 102(49):17792–17797. [PubMed: 16314561]

Cornell RA, Eisen JS. Notch in the pathway: the roles of Notch signaling in neural crest development. Semin Cell Dev Biol. 2005; 16(6):663–672. [PubMed: 16054851]

Davis JA, Reed RR. Role of Olf-1 and Pax-6 transcription factors in neurodevelopment. J Neurosci. 1996; 16(16):5082–5094. [PubMed: 8756438]

Deneen B, Ho R, Lukaszewicz A, Hochstim CJ, Gronostajski RM, Anderson DJ. The transcription factor NFIA controls the onset of gliogenesis in the developing spinal cord. Neuron. 2006; 52(6): 953–968. [PubMed: 17178400]

Eckler MJ, McKenna WL, Taghvaei S, McConnell SK, Chen B. Fezf1 and Fezf2 are required for olfactory development and sensory neuron identity. J Comp Neurol. 2011; 519(10):1829–1846. [PubMed: 21452247]

Farkas LM, Huttner WB. The cell biology of neural stem and progenitor cells and its significance for their proliferation versus differentiation during mammalian brain development. Curr Opin Cell Biol. 2008; 20(6):707–715. [PubMed: 18930817]

Fietz SA, Kelava I, Vogt J, Wilsch-Brauninger M, Stenzel D, Fish JL, Corbeil D, Riehn A, Distler W, Nitsch R, Huttner WB. OSVZ progenitors of human and ferret neocortex are epithelial-like and expand by integrin signaling. Nat Neurosci. 2010; 13(6):690–699. [PubMed: 20436478]

Gaiano N, Nye JS, Fishell G. Radial glial identity is promoted by Notch1 signaling in the murine forebrain. Neuron. 2000; 26(2):395–404. [PubMed: 10839358]

Gómez-López S, Wiskow O, Favaro R, Nicolis SK, Price DJ, Pollard SM, Smith A. Sox2 and Pax6 maintain the proliferative and developmental potential of gliogenic neural stem cells In vitro. Glia. 2011; 59(11):1588–1599. [PubMed: 21766338]

Gotz M, Stoykova A, Gruss P. Pax6 controls radial glia differentiation in the cerebral cortex. Neuron. 1998; 21(5):1031–1044. [PubMed: 9856459]

Guillemot F. Cell fate specification in the mammalian telencephalon. Prog Neurobiol. 2007; 83(1):37–52. [PubMed: 17517461]

Hansen DV, Lui JH, Parker PR, Kriegstein AR. Neurogenic radial glia in the outer subventricular zone of human neocortex. Nature. 2010; 464(7288):554–561. [PubMed: 20154730]

Haubensak W, Attardo A, Denk W, Huttner WB. Neurons arise in the basal neuroepithelium of the early mammalian telencephalon: a major site of neurogenesis. Proc Natl Acad Sci U S A. 2004; 101(9):3196–3201. [PubMed: 14963232]

Heng YH, Barry G, Richards LJ, Piper M. Nuclear factor I genes regulate neuronal migration. Neurosignals. 2012; 20(3):159–167. [PubMed: 22456058]

Hevner RF, Haydar TF. The (not necessarily) convoluted role of basal radial glia in cortical neurogenesis. Cereb Cortex. 2012; 22(2):465–468. [PubMed: 22116731]

Hevner RF, Hodge RD, Daza RAM, Englund C. Transcription factors in glutamatergic neurogenesis: Conserved programs in neocortex, cerebellum, and adult hippocampus. Neuroscience Research. 2006; 55(3):223–233. [PubMed: 16621079]

Hsu F, Kent WJ, Clawson H, Kuhn RM, Diekhans M, Haussler D. The UCSC Known Genes. Bioinformatics. 2006; 22(9):1036–1046. [PubMed: 16500937]

Huang DW, Sherman BT, Lempicki RA. Bioinformatics enrichment tools: paths toward the comprehensive functional analysis of large gene lists. Nucleic Acids Research. 2009a; 37(1):1–13. [PubMed: 19033363]

Huang DW, Sherman BT, Lempicki RA. Systematic and integrative analysis of large gene lists using DAVID Bioinformatics Resources. Nature Protocols. 2009b; 4(1):44–57.

Imayoshi I, Sakamoto M, Yamaguchi M, Mori K, Kageyama R. Essential roles of Notch signaling in maintenance of neural stem cells in developing and adult brains. J Neurosci. 2011; 30(9):3489–3498. [PubMed: 20203209]

Jacobs EC, Campagnoni C, Kampf K, Reyes SD, Kalra V, Handley V, Xie YY, Hong-Hu Y, Spreur V, Fisher RS, Campagnoni AT. Visualization of corticofugal projections during early cortical development in a tau-GFP-transgenic mouse. Eur J Neurosci. 2007; 25(1):17–30. [PubMed: 17241263]

Joshi PS, Molyneaux BJ, Feng L, Xie X, Macklis JD, Gan L. Bhlhb5 regulates the postmitotic acquisition of area identities in layers II–V of the developing neocortex. Neuron. 2008; 60(2):258–272. [PubMed: 18957218]

Kowalczyk T, Pontious A, Englund C, Daza RA, Bedogni F, Hodge R, Attardo A, Bell C, Huttner WB, Hevner RF. Intermediate neuronal progenitors (basal progenitors) produce pyramidal-projection neurons for all layers of cerebral cortex. Cereb Cortex. 2009; 19(10):2439–2450. [PubMed: 19168665]

Kumbasar A, Plachez C, Gronostajski RM, Richards LJ, Litwack ED. Absence of the transcription factor Nfib delays the formation of the basilar pontine and other mossy fiber nuclei. J Comp Neurol. 2009; 513(1):98–112. [PubMed: 19107796]

Kwan KY, Lam MM, Krsnik Z, Kawasawa YI, Lefebvre V, Sestan N. SOX5 postmitotically regulates migration, postmigratory differentiation, and projections of subplate and deep-layer neocortical neurons. Proc Natl Acad Sci U S A. 2008; 105(41):16021–16026. [PubMed: 18840685]

Langmead B, Trapnell C, Pop M, Salzberg SL. Ultrafast and memory-efficient alignment of short DNA sequences to the human genome. Genome Biol. 2009; 10(3):R25. [PubMed: 19261174]

Leone DP, Srinivasan K, Chen B, Alcamo E, McConnell SK. The determination of projection neuron identity in the developing cerebral cortex. Curr Opin Neurobiol. 2008; 18(1):28–35. [PubMed: 18508260]

Li H, Handsaker B, Wysoker A, Fennell T, Ruan J, Homer N, Marth G, Abecasis G, Durbin R. The Sequence Alignment/Map format and SAMtools. Bioinformatics. 2009; 25(16):2078–2079. [PubMed: 19505943]

Louvi A, Artavanis-Tsakonas S. Notch signalling in vertebrate neural development. Nat Rev Neurosci. 2006; 7(2):93–102. [PubMed: 16429119]

Lui JH, Hansen DV, Kriegstein AR. Development and evolution of the human neocortex. Cell. 2011; 146(1):18–36. [PubMed: 21729779]

Mason S, Piper M, Gronostajski R, Richards L. Nuclear Factor One Transcription Factors in CNS Development. Molecular Neurobiology. 2009; 39(1):10–23. [PubMed: 19058033]

McConnell SK. Constructing the cerebral cortex: neurogenesis and fate determination. Neuron. 1995; 15(4):761–768. [PubMed: 7576626]

McKenna WL, Betancourt J, Larkin KA, Abrams B, Guo C, Rubenstein JL, Chen B. Tbr1 and Fezf2 regulate alternate corticofugal neuronal identities during neocortical development. J Neurosci. 2011; 31(2):549–564. [PubMed: 21228164]

Molyneaux BJ, Arlotta P, Hirata T, Hibi M, Macklis JD. Fezl Is Required for the Birth and Specification of Corticospinal Motor Neurons. Neuron. 2005; 47(6):817–831. [PubMed: 16157277]

Molyneaux BJ, Arlotta P, Menezes JRL, Macklis JD. Neuronal subtype specification in the cerebral cortex. Nat Rev Neurosci. 2007; 8(6):427–437. [PubMed: 17514196]

Noctor SC, Martinez-Cerdeno V, Ivic L, Kriegstein AR. Cortical neurons arise in symmetric and asymmetric division zones and migrate through specific phases. Nat Neurosci. 2004; 7(2):136–144. [PubMed: 14703572]

Noctor SC, Martinez-Cerdeno V, Kriegstein AR. Neural stem and progenitor cells in cortical development. Novartis Found Symp. 2007; 288:59–73. discussion 73–58, 96–58. [PubMed: 18494252]

Noctor SC, Martinez-Cerdeno V, Kriegstein AR. Distinct behaviors of neural stem and progenitor cells underlie cortical neurogenesis. J Comp Neurol. 2008; 508(1):28–44. [PubMed: 18288691]

Piper M, Barry G, Hawkins J, Mason S, Lindwall C, Little E, Sarkar A, Smith AG, Moldrich RX, Boyle GM, Tole S, Gronostajski RM, Bailey TL, Richards LJ. NFIA controls telencephalic progenitor cell differentiation through repression of the Notch effector Hes1. J Neurosci. 2010; 30(27):9127–9139. [PubMed: 20610746]

Piper M, Moldrich R, Lindwall C, Little E, Barry G, Mason S, Sunn N, Kurniawan N, Gronostajski R, Richards L. Multiple non-cell-autonomous defects underlie neocortical callosal dysgenesis in Nfib-deficient mice. Neural Development. 2009; 4(1):43. [PubMed: 19961580]

Plachez C, Lindwall C, Sunn N, Piper M, Moldrich RX, Campbell CE, Osinski JM, Gronostajski RM, Richards LJ. Nuclear factor I gene expression in the developing forebrain. The Journal of Comparative Neurology. 2008; 508(3):385–401. [PubMed: 18335562]

Reillo I, de Juan Romero C, Garcia-Cabezas MA, Borrell V. A role for intermediate radial glia in the tangential expansion of the mammalian cerebral cortex. Cereb Cortex. 2011; 21(7):1674–1694. [PubMed: 21127018]

Saito T. NEPRO: a novel Notch effector for maintenance of neural progenitor cells in the neocortex. Adv Exp Med Biol. 2012; 727:61–70. [PubMed: 22399339]

Schaeren-Wiemers N, Gerfin-Moser A. A single protocol to detect transcripts of various types and expression levels in neural tissue and cultured cells: in situ hybridization using digoxigenin-labelled cRNA probes. Histochemistry. 1993; 100(6):431–440. [PubMed: 7512949]

Sessa A, Mao CA, Hadjantonakis AK, Klein WH, Broccoli V. Tbr2 directs conversion of radial glia into basal precursors and guides neuronal amplification by indirect neurogenesis in the developing neocortex. Neuron. 2008; 60(1):56–69. [PubMed: 18940588]

Shitamukai A, Konno D, Matsuzaki F. Oblique radial glial divisions in the developing mouse neocortex induce self-renewing progenitors outside the germinal zone that resemble primate outer subventricular zone progenitors. J Neurosci. 2011; 31(10):3683–3695. [PubMed: 21389223]

Shitamukai A, Matsuzaki F. Control of asymmetric cell division of mammalian neural progenitors. Dev Growth Differ. 2012; 54(3):277–286. [PubMed: 22524601]

Smit, AFA.; Hubley, R.; Green, P. Repeat Masker Open-3.0. 1996–2010. http://www.repeatmasker.org

Steele-Perkins G, Plachez C, Butz KG, Yang G, Bachurski CJ, Kinsman SL, Litwack ED, Richards LJ, Gronostajski RM. The Transcription Factor Gene Nfib Is Essential for both Lung Maturation and Brain Development. Molecular and Cellular Biology. 2005; 25(2):685–698. [PubMed: 15632069]

Struikmans H, Rutgers DH, Jansen GH, Tulleken CA, van der Tweel I, Battermann JJ. S-phase fraction, 5-bromo-2′-deoxy-uridine labelling index, duration of S-phase, potential doubling time, and DNA index in benign and malignant brain tumors. Radiat Oncol Investig. 1997; 5(4):170–179.

Tarabykin V, Stoykova A, Usman N, Gruss P. Cortical upper layer neurons derive from the subventricular zone as indicated by Svet1 gene expression. Development. 2001; 128(11):1983–1993. [PubMed: 11493521]

Taupin P. BrdU immunohistochemistry for studying adult neurogenesis: paradigms, pitfalls, limitations, and validation. Brain Res Rev. 2007; 53(1):198–214. [PubMed: 17020783]

Tiberi L, Vanderhaeghen P, van den Ameele J. Cortical neurogenesis and morphogens: diversity of cues, sources and functions. Curr Opin Cell Biol. 2012; 24(2):269–276. [PubMed: 22342580]

Trapnell C, Pachter L, Salzberg SL. TopHat: discovering splice junctions with RNA-Seq. Bioinformatics. 2009; 25(9):1105–1111. [PubMed: 19289445]

Wang W, Mullikin-Kilpatrick D, Crandall JE, Gronostajski RM, Litwack ED, Kilpatrick DL. Nuclear Factor I Coordinates Multiple Phases of Cerebellar Granule Cell Development via Regulation of Cell Adhesion Molecules. Journal of Neuroscience. 2007; 27(23):6115–6127. [PubMed: 17553984]

Wang X, Lui JH, Kriegstein AR. Orienting fate: spatial regulation of neurogenic divisions. Neuron. 2011b; 72(2):191–193. [PubMed: 22017981]

Wang X, Tsai JW, LaMonica B, Kriegstein AR. A new subtype of progenitor cell in the mouse embryonic neocortex. Nat Neurosci. 2011a; 14(5):555–561. [PubMed: 21478886]

Yoon K, Gaiano N. Notch signaling in the mammalian central nervous system: insights from mouse mutants. Nat Neurosci. 2005; 8(6):709–715. [PubMed: 15917835]

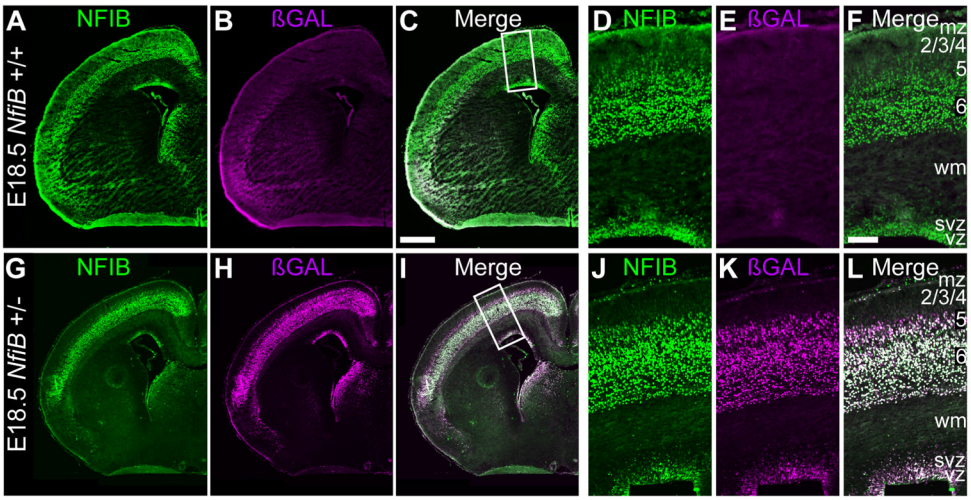


**Figure 1.**

βGAL expression recapitulates NFIB expression in the cerebral cortex. Immunohistochemistry and confocal microscopy were used to determine expression of βGAL and NFIB expression in coronal sections of E18.5 *NfiB*$^{+/+}$ (**A–F**) and *NfiB*$^{+/-}$ (**G–L**) brains. NFIB was expressed in deep cortical layers, 5 and 6, and proliferative zone of *NfiB*$^{+/+}$ (**A, D)** and *NfiB*$^{+/-}$ (**G, J**) cortices. βGAL was not expressed in *NfiB*$^{+/+}$ **(B, E)** cortices, and therefore did not coincide with NFIB expression (**C, F**). In *NfiB*$^{+/-}$ cortices, βGAL expression was restricted to nearly all NFIB-expressing cells in deep cortical layers and proliferative zones (**H, K**; Merge **I, L**), thus validating the use of GAL immunostaining in identifying NFIB-expressing cells in *NfiB*$^{+/-}$ cortices. **A–C**, **G–I** Low magnification; scale bar, 500μm. **D–F**, **J–L** show boxed regions in **C** and **I**, respectively; scale bar, 100μm.

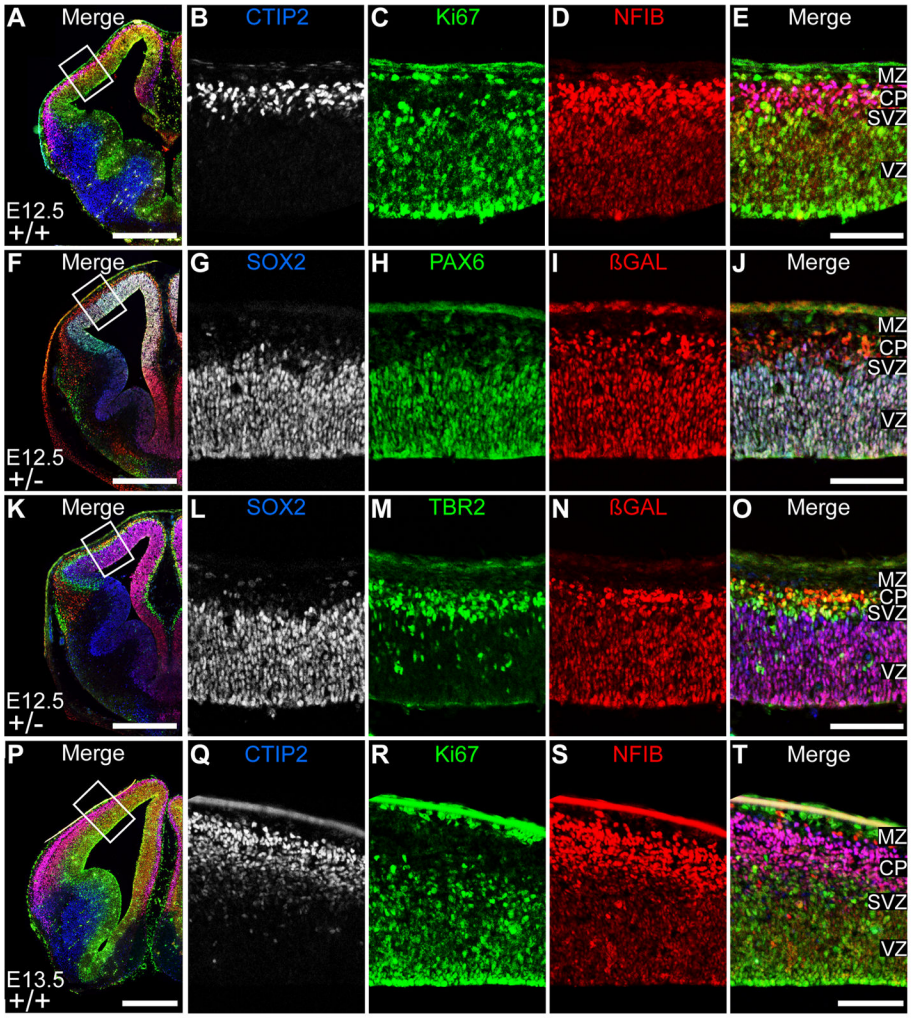

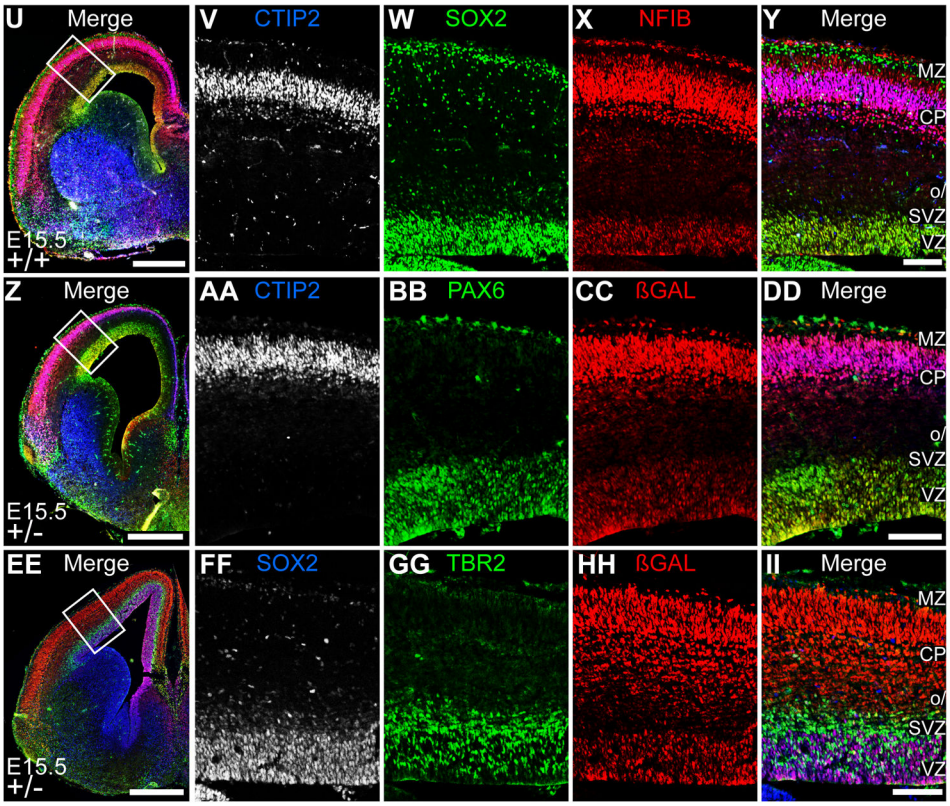


**Figure 2.**

NFIB is expressed in neural progenitors and deep layer neurons throughout cortical development. Immunohistochemistry and confocal microscopy were used to determine cell-type specific expression of NFIB and βGAL in coronal sections of *NfiB*$^{+/+}$ (**A–E, P–T, U–Y**) and *NfiB*$^{+/-}$ (**F–O, Z–II**) brains, respectively. A–O, E12.5; P–T, E13.5; U–II, E15.5. **A, F, K, P, U, Z, EE** Low magnification; scale bars, 500μm. **B–E, G–J, L–O, Q–T, V–Y, AA–DD, EE–II** show boxed regions (**A, F, K, P, U**, **Z, EE**, respectively); scale bars, 100μm.

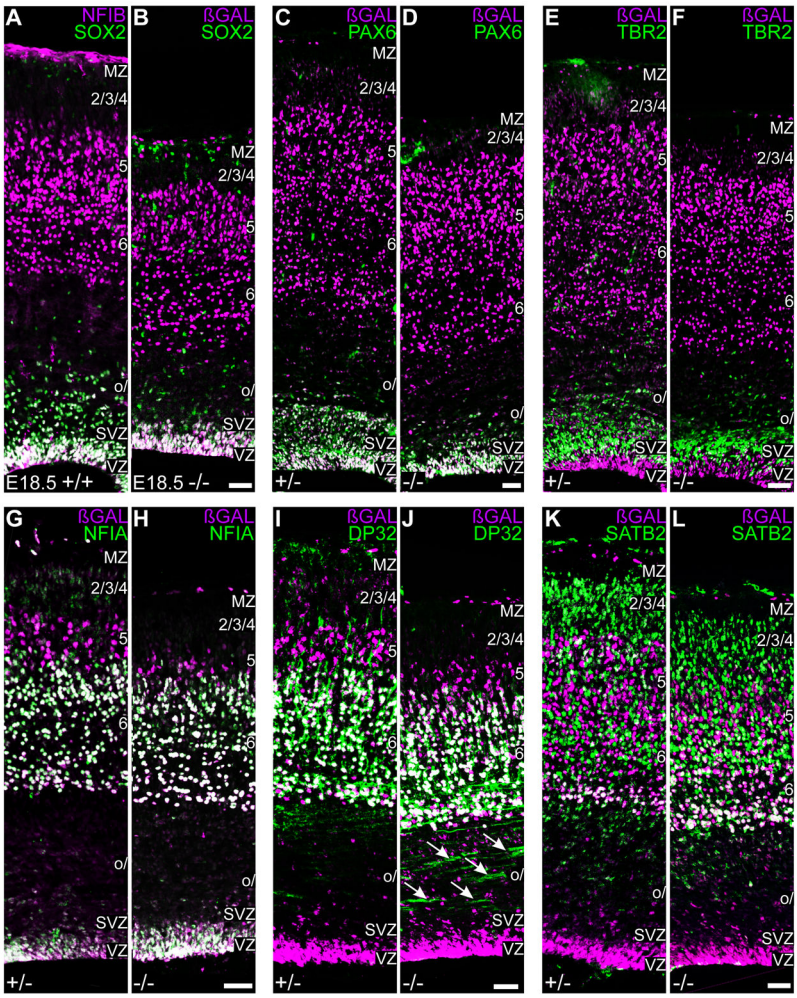


**Figure 3.**

The molecular identity of *NfiB* mutant cells is similar to NFIB-expressing cells. Immunohistochemistry and fluorescent microscopy were used to compare the molecular marker identities of NFIB or βGAL expressing cells in coronal sections of $NfiB^{-/-}$ and $NfiB^{+/+}$ or $NfiB^{+/-}$ cortices at E18.5. **A–B** Expression of NFIB (magenta, **A**) or βGAL (magenta, **B**) and SOX2 (green) in $NfiB^{+/+}$ (**A**) and $NfiB^{-/-}$ (**B**) cortices, respectively. **C–L** Expression of βGAL (magenta) and PAX6 (**B–C**), TBR2 (**D–E**), NFIA (**G–H**), DARPP32 (denoted as DP32, **I–J**) or SATB2 (**K–L**) (all in green) in $NfiB^{+/-}$ (**C, E, G, I** and **K**) and $NfiB^{-/-}$ (**D, F, H, J, L**) cortices. Scale bars, 25μm.

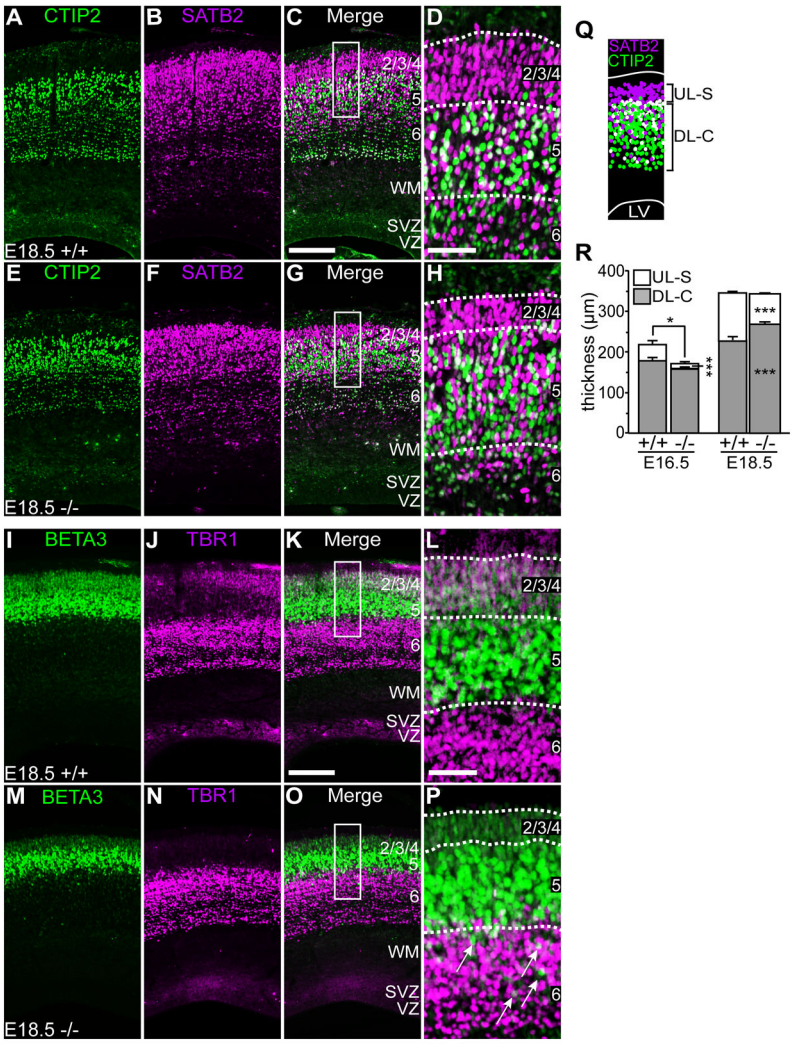


**Figure 4.**

Severe thinning of upper cortical layers in *NfiB*$^{-/-}$ mice. Immunohistochemistry and confocal microscopy were used to compare overall cortical lamination and expression of specific neuronal makers in *NfiB*$^{+/+}$ (**A–D, I–L, Q–R**) versus *NfiB*$^{-/-}$ (**E–H, M–R**) brains at E18.5. **A–H** Expression of CTIP2 and SATB2 in *NfiB*$^{+/+}$ and *NfiB*$^{-/-}$ cortices. **I–P** Expression of BETA3 and TBR1 in *NfiB*$^{+/+}$ and *NfiB*$^{-/-}$ cortices. Arrows (in **P**) point to BETA3-expressing cells in layer 6. **A–C, E–G, I–K, M–O** scale bar, 100µm. **D, H, L** and **P** show boxed region in **C, G, K** and **O**, respectively; dashed lines indicate estimated boundaries between cortical layers; scale bar, 50µm. **Q** Schematic shows definitions of regions containing upper layer SATB2$^{+}$ neurons (UL-S) and deep layer CTIP2$^{+}$ neurons (DL-C); see materials and methods for details. **R** Graph showing comparison of UL-S and DL-C thickness (µm) between *NfiB*$^{+/+}$ and *NfiB*$^{-/-}$ mice at E16.5 and E18.5. *p = 0.0077, ***p ≤ 0.0001 by t-test; n = 12 matched sections/age, 4 mice/genotype; error bars indicate SEM.

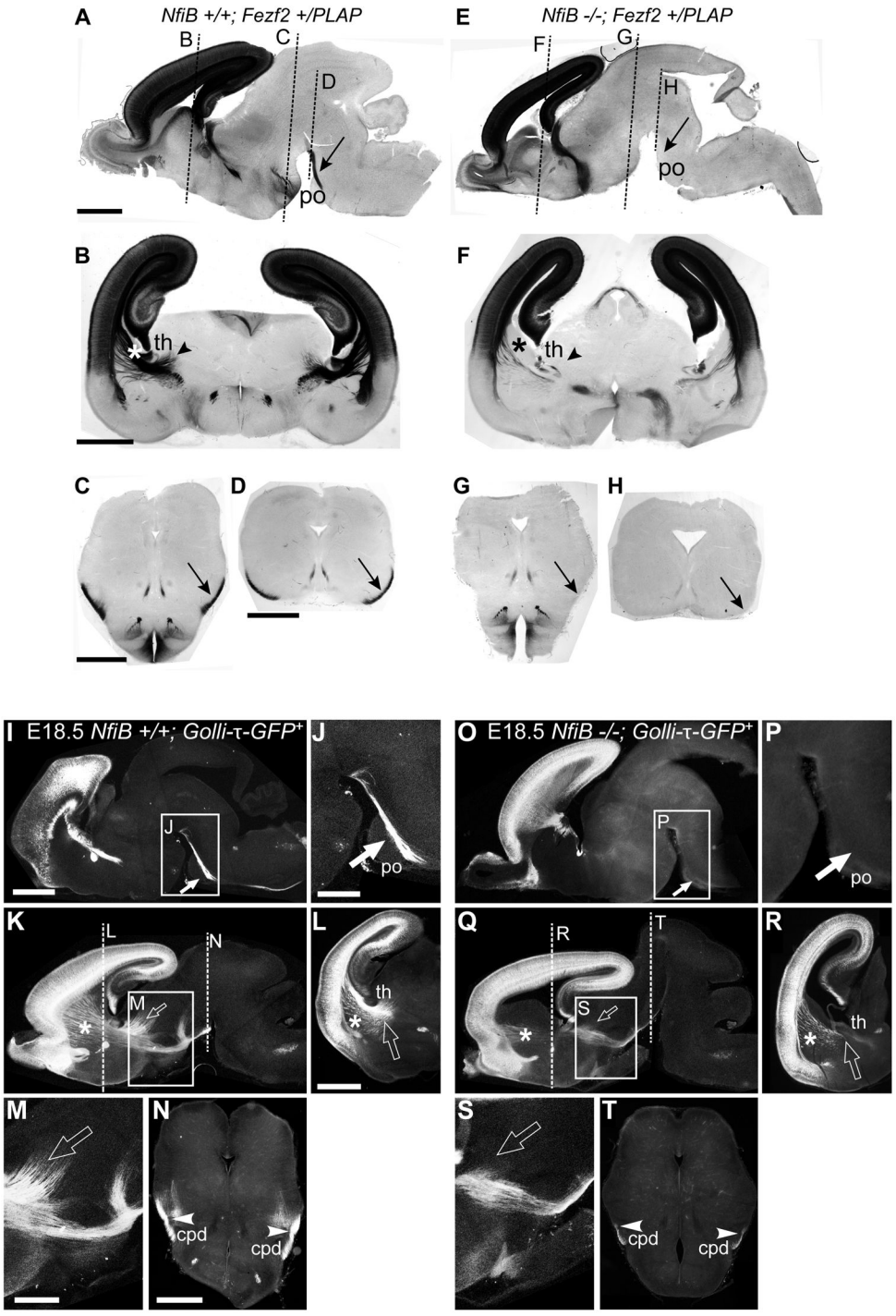


**Figure 5.**

*NfiB*$^{-/-}$ mice display a significant loss of corticofugal axonal projections. **A–H** PLAP-staining and bright field microscopy were used to identify PLAP-labeled (black) corticofugal axon tracts in *NfiB*$^{+/+}$*; Fezf2*$^{+/PLAP}$ (**A–D)** and *NfiB*$^{-/-}$; *Fezf2*$^{+/PLAP}$ (**E–H**) brains at E18.5. Sagittal sections (**A, E**) with dashed lines indicating approximate anterior-posterior location of coronal images displayed below (**B–D, F–H**, respectively). **I–T**

Immunohistochemistry and fluorescent microscopy were used to identify GFP-labeled (white) corticofugal axon tracts in *NfiB*$^{+/+}$*; Golli-τ-GFP*$^{+}$ (**I–N**) and *NfiB*$^{-/-}$*; Golli-τ-GFP*$^{+}$ (**O–T**) brains at E18.5. **I–N** Sagittal (**I, J, K, M**) and coronal (**L, N)** views of subcerebral (**I** and **J**, **N**) and corticothalamic (**K** and **M, L**) tracts. Dashed lines in **K** and **Q** indicate approximate anterior-posterior location of coronal images (**L** and **N**, **R** and **T**, respectively). Black arrows (**A, C, D, E, G, H**) point to cerebral peduncle, black arrowheads (**B, F**) point to the thalamus. White arrows point to corticospinal tract through pons (**I, J**) or reduction thereof (**O, P**); open arrows point to corticothalamic tract (**K–M**) or reduction thereof (**Q–S**); asterisks (**B, F, K, L, Q** and **R**) indicate internal capsule; white arrowheads point to corticospinal tract through cerebral peduncle (**N**) or reduction thereof (**T**). **A–H, I, K, L, N, O, Q, R, T** Low magnification; scale bars, 1000μm. **J, M, P, S** show boxed region (**I, K, O, Q,** respectively); scale bars, 500μm. po, Pons; th, thalamus; cpd, cerebral peduncle Scale bars, 1000μm.

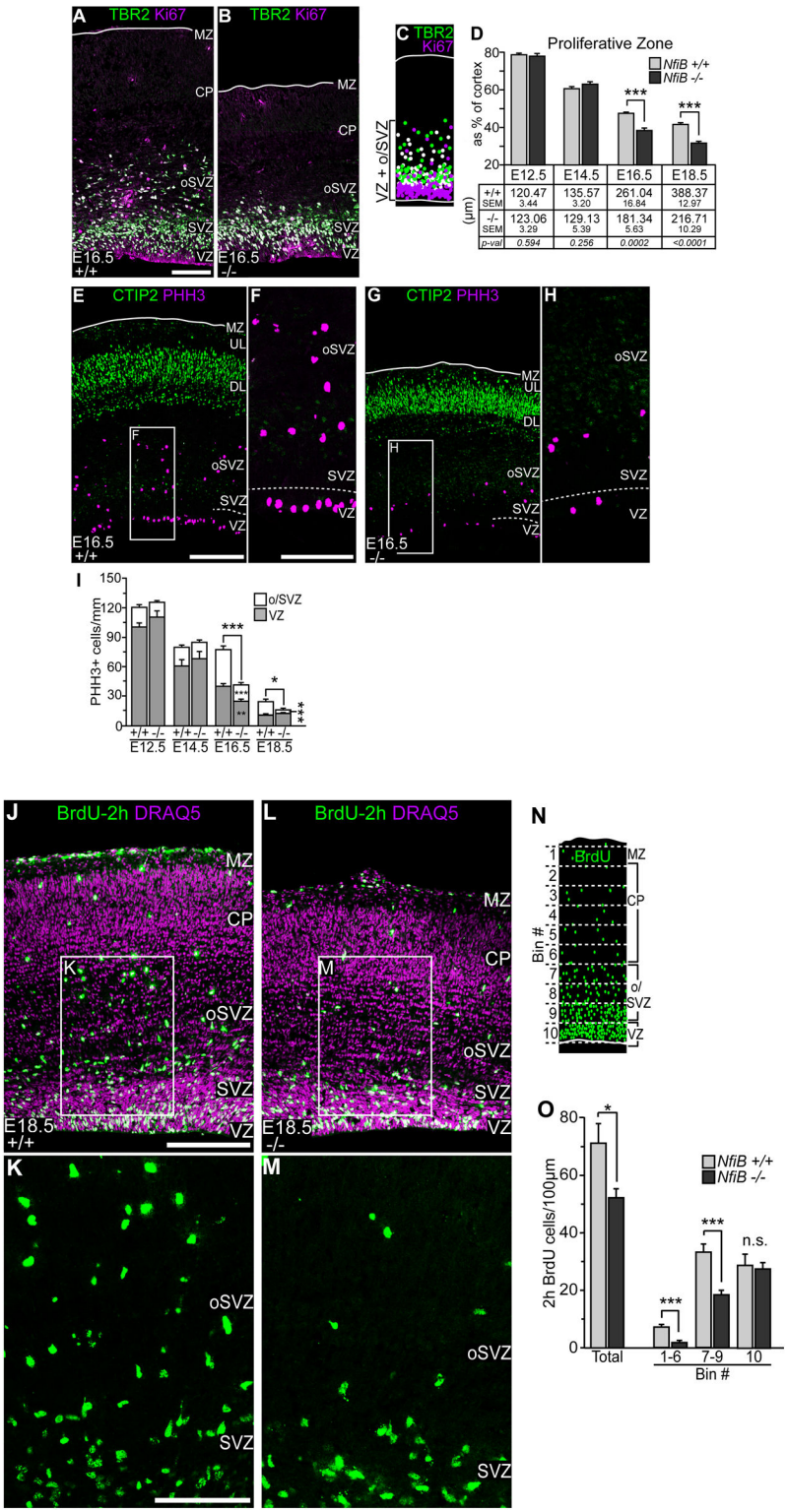


**Figure 6.**

Loss of actively dividing neural progenitors during late corticogenesis.

Immunohistochemistry and confocal microscopy were used to quantify and analyze the

distribution of proliferating cells in coronal sections of *NfiB*$^{+/+}$ and *NfiB*$^{-/-}$ brains throughout cortical development. **A–D,** Expression of TBR2 (green) and Ki67 (magenta) in *NfiB*$^{+/+}$ (**A**) and *NfiB*$^{-/-}$ (**B**) cortices at E16.5. **C** Schematic showing definition of the proliferative zone (V + o/SVZ); see materials and methods for details. **D** Graph and table representing V + o/SVZ thickness as both a percentage of total cortical thickness and as absolute value (μm) in *NfiB*$^{+/+}$ and *NfiB*$^{-/-}$ mice at E12.5, E14.5, E16.5 and E18.5. ***p = 0.0004 (E16.5), ***p < 0.0001 (E18.5). **E–I** Expression of CTIP2 (green) and PHH3 (magenta) in *NfiB*$^{+/+}$ (**E, F**) and *NfiB*$^{-/-}$ (**G, H**) cortices at E16.5. **I,** Graph showing comparison of the number of PHH3-expressing cells/mm in VZ and o/SVZ (and total number) between *NfiB*$^{+/+}$ and *NfiB*$^{-/-}$ mice. *p = 0.0263, **p = 0.0044, ***p = 0.0001. **J–O** BrdU-labeled cells (green) and DRAQ5 nuclear stain (magenta) in E18.5 *NfiB*$^{+/+}$ (**J, K**) and *NfiB*$^{-/-}$ (**L, M**) cortices, 2 hours post BrdU-labeling. **N,** Schematic showing analysis of cortical distribution of BrdU-labeled cells by binning; see Materials and Methods for details. **O** Number of total BrdU-labeled cells/100μm and in bins 1–6, 7–9 and 10 was compared between E18.5 *NfiB*$^{+/+}$ and *NfiB*$^{-/-}$ cortices. *p = 0.0267, ***p < 0.0001. Statistical analyses by t-test, error bars represent SEM; n = 12 matched sections/age, 4 mice/genotype (graphs **D, I, O**). **A, B, E, G, J, L** scale bars, 100μm. **F, H, K, M** show boxed regions in **E, G, J, L**, respectively; scale bar 50μm.

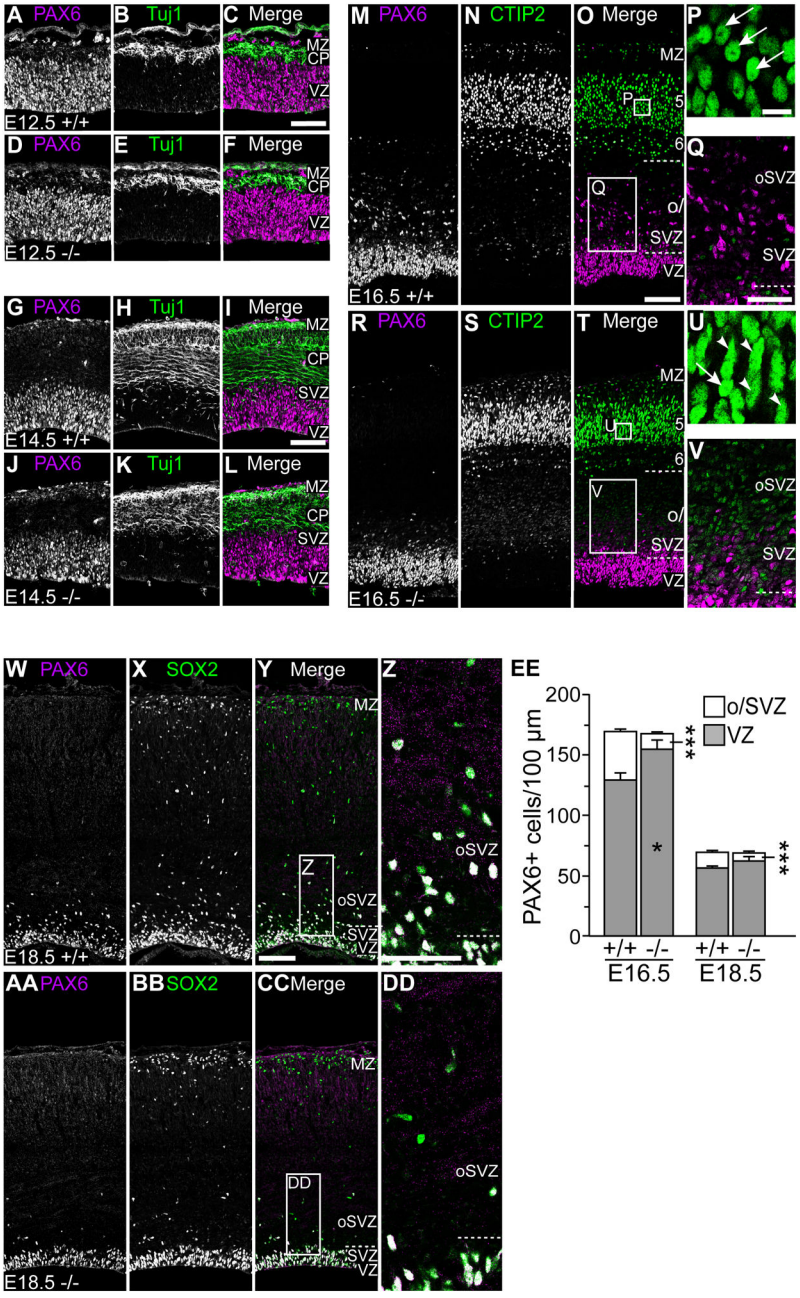


**Figure 7.**

*NfiB*$^{-/-}$ brains display a major loss of outer radial glia during late corticogenesis. Immunohistochemistry and confocal microscopy of coronal brain sections were used to compare the quantity and distribution of PAX6-expressing cells in *NfiB*$^{+/+}$ and *NfiB*$^{-/-}$ mice throughout cortical development. **A–F** PAX6 (magenta) and Tuj1 (green) expression in E12.5 *NfiB*$^{+/+}$ (**A–C**) and *NfiB*$^{-/-}$ (**D–F**) cortices. **G–L** PAX6 (magenta) and Tuj1 (green) expression in E14.5 *NfiB*$^{+/+}$ (**G–I**) and *NfiB*$^{-/-}$ (**J–L**) cortices. **M–V** PAX6 (magenta) and CTIP2 (green) expression in E16.5 *NfiB*$^{+/+}$ (**M–Q**) and *NfiB*$^{-/-}$ (**R–V**) cortices. Arrows (**P, U**) point to CTIP2$^{+}$ cells with rounded morphology; arrowheads (**U**) point to CTIP2$^{+}$ cells

with elongated morphology; dashed lines (**O, Q, T, V**) indicate D–V boundaries of o/SVZ. **W–DD** PAX6 (magenta) and SOX2 (green) expression in E18.5 *NfiB*$^{+/+}$ (**W–Z**) and *NfiB*$^{-/-}$ (**AA–DD**). Dashed lines (**Y, Z, CC, DD**) indicate approximate border between SVZ and oSVZ. **A–O, R–T, W–Y, AA–CC** scale bars, 100μm. **P** and **U** show boxed regions in layer 5 of **O** and **T**, respectively; scale bars, 10μm. **Q** and **V** show boxed regions in o/SVZ in **O** and **T** respectively; scale bars, 50μm. **Z** and **DD** show boxed regions in **Y** and **CC,** respectively; scale bars 25μm. **EE,** Total number of PAX6$^{+}$ cells/100μm and in VZ, o/SVZ were compared between *NfiB*$^{+/+}$ and *NfiB*$^{-/-}$ mice at E16.5, and E18.5. *p = 0.0461, ***p < 0.0001 by t-test, error bars represent SEM; n = 10 matched sections/age, 4 mice/genotype.

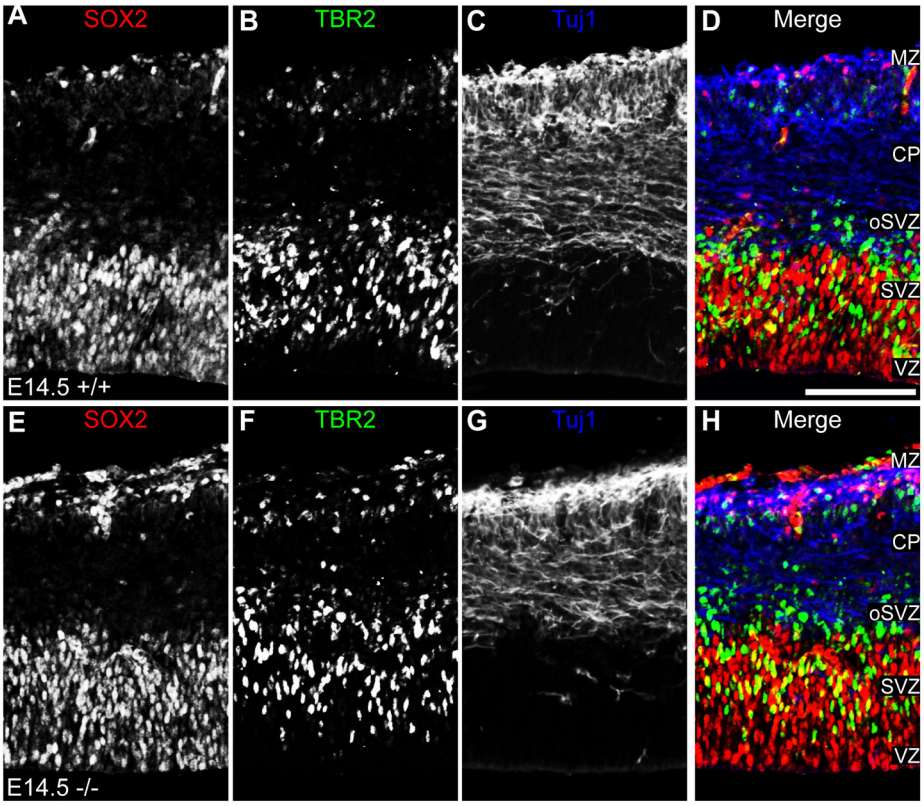

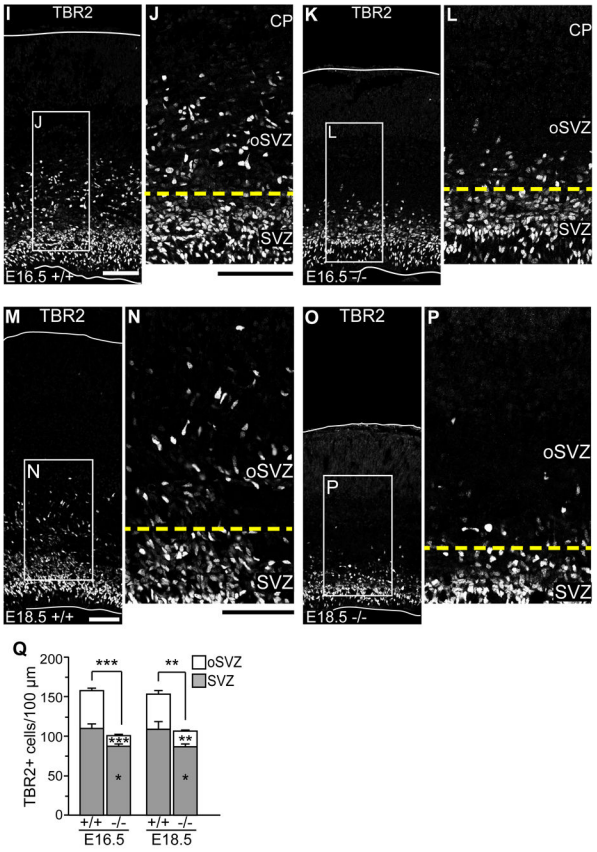


**Figure 8.**

Loss of basal progenitors in *NfiB*$^{-/-}$ brains during late coticogenesis. Immunohistochemistry and confocal microscopy of coronal brain sections were used to compare the number and distribution of TBR2-expressing cells in *NfiB*$^{+/+}$ and *NfiB*$^{-/-}$ mice throughout cortical development. **A–H** SOX2 (red, **A, E**), TBR2 (green, **B, F**) and Tuj1 (blue, **C, G**) expression (Merge **D, H**) in *NfiB*$^{+/+}$ (**A–D**) and *NfiB*$^{-/-}$ (**E–H**) cortices at E14.5. **I–L** TBR2 expression in *NfiB*$^{+/+}$ (**I, J, M, N**) and *NfiB*$^{-/-}$ (**K, L, O, P**) at E16.5 (**I–L**) and E18.5 (**M–P**). White outlines (**I, K, M, O**) indicate apical and basal surfaces of the cortex, yellow dashed lines (J, L, N, P) indicate approximate boundary between SVZ and oSVZ. **J, L, N,** and **P** show boxed regions in **I, K, M** and **O,** respectively. Scale bars, 100µm. **Q** Total numbers of TBR2$^{+}$ cells/100µm and in VZ and o/SVZ were compared between *NfiB*$^{+/+}$ and *NfiB*$^{-/-}$ mice at E16.5, and E18.5. *p = 0.0095 (E16.5), *p = 0.0429 (E18.5), **p = 0.0011 (E18.5 oSVZ), **p = 0.0028 (E18.5 total number), ***p < 0.0001 by t-test, error bars indicate SEM; n = 9 matched sections/age, 4 mice/genotype.

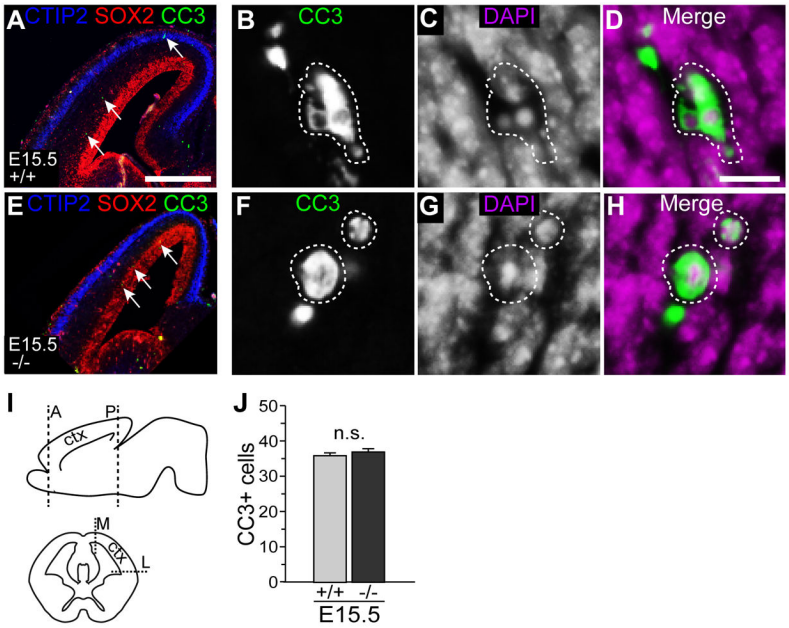


**Figure 9.**

Number of apoptotic cells is similar in *NfiB*$^{+/+}$ and *NfiB*$^{-/-}$ cortices at E15.5. Immunohistochemistry and confocal microscopy of coronal brain sections were used to quantify CC3$^{+}$ cells in *NfiB*$^{+/+}$ and *NfiB*$^{-/-}$ mice at E15.5. **A, E** Low magnification view of CTIP2 (blue), SOX2 (red) and CC3 (green) expression in *NfiB*$^{+/+}$ (**A**) and *NfiB*$^{-/-}$ (**E**) cortices; arrows point to CC3-expressing cells. **B–D, F–H** Higher magnification view of CC3 (green) and DAPI nuclear stain (magenta) expression (**B, F** and **C, G**, respectively, Merge **D, F**) in *NfiB*$^{+/+}$ (**B–D**) and *NfiB*$^{-/-}$ (**F–H**) cortices; CC3$^{+}$ cells are indicated by dashed outlines. **A, E** scale bars, 500μm; **B–D, F–H** scale bars, 10μm. **I** Schematics showing regions of CC3$^{+}$ cell quantification. Coronal sections within anterior (A) to posterior (P) region indicated by dashed lines (top panel) were used; CC3$^{+}$ cells were quantified on the medial (M) to lateral (L) axis within region indicated by dashed lines (bottom panel); ctx, cortex. **J** Number of CC3$^{+}$ cells was compared between *NfiB*$^{+/+}$ and *NfiB*$^{-/-}$ cortices at E15.5. p = 0.379 by t-test, error bars indicate SEM; n=10 matched sections, 4 mice/genotype.

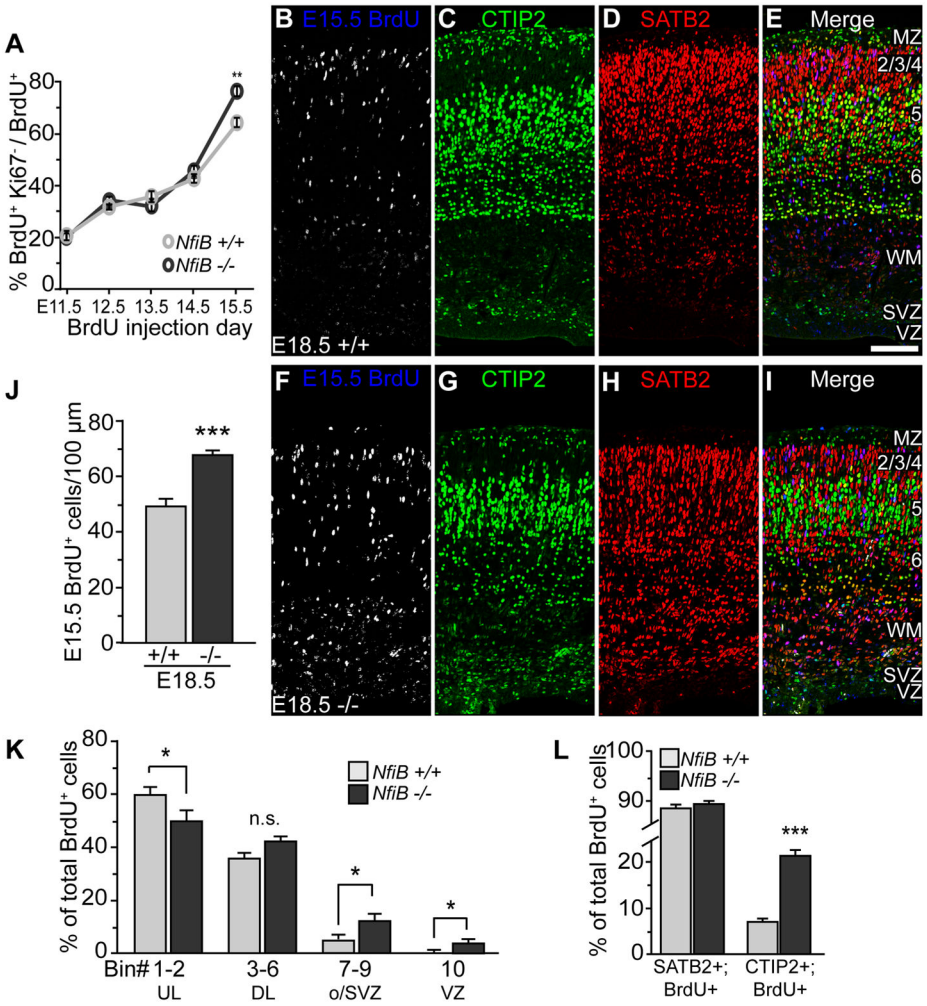


**Figure 10.**

Increase in neurogenesis at E15.5 and defects in neuronal migration. Immunohistochemistry and confocal microscopy of coronal brain sections were used to compare the quit fractions throughout neurogenesis and molecular identities of neurons born at E15.5 in $NfiB^{+/+}$ and $NfiB^{-/-}$ cortices. **A** Quit fractions in $NfiB^{+/+}$ and $NfiB^{-/-}$ mice at E11.5–E15.5. **p = 0.0045 by t-test, error bars indicate SEM; n = 9 matched sections/age, 3 mice/genotype. **B–L** BrdU labeling was used to quantify and analyze the distribution of neurons generated at E15.5 in $NfiB^{+/+}$ and $NfiB^{-/-}$ cortices; combining with SATB2 and CTIP2 immunostaining (**B—** and **L**) allowed for analysis of neuronal marker expression. **B–I** E15.5 $BrdU^+$ cells (**B, F**) and expression of CTIP2 and SATB2 (**C, G** and **D, H**, respectively, Merge **E, I**) in E18.5 $NfiB^{+/+}$ (**B–E**) and $NfiB^{-/-}$ (**F–I**) cortices; scale bar, 100µm. **J** Total number of E15.5 $BrdU^+$ cells/100µm was compared between $NfiB^{+/+}$ and $NfiB^{-/-}$ cortices; ***p = 0.0001. **K** The cortical distribution of E15.5 $BrdU^+$ cells was analyzed by binning; see Materials and Methods for details. E15.5 $BrdU^+$ cells in bins 1–2, 3–6, 7–9 and 10 as a percentage of total number were compared between $NfiB^{+/+}$ and $NfiB^{-/-}$ cortices. *p = 0.038, *p = 0.0287, *p = 0.0066 (bins 1–2, 7–9 and 10, respectively). **L** Percentages of total E15.5 $BrdU^+$ cells that expressed either SATB2 or CTIP2 were compared between $NfiB^{+/+}$ and $NfiB^{-/-}$ cortices.

***p <0.0001. **J–L** p-values calculated by t-test, error bars indicate SEM; n = 12 matched sections, 4 brains/genotype.

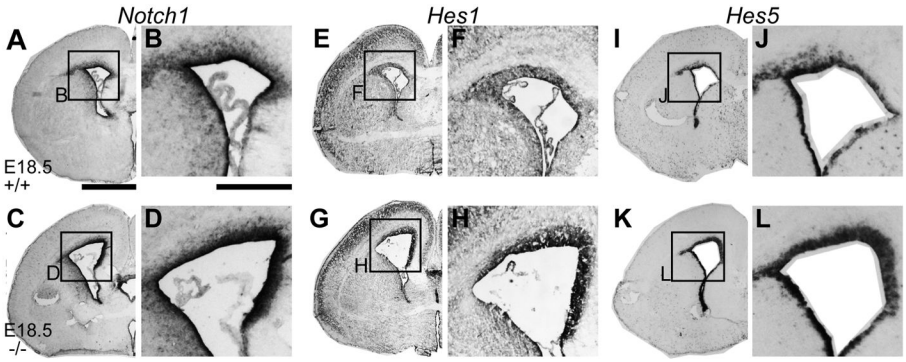


**Figure 11.**

mRNA expression of *Notch* signaling pathway members is upregulated in *NfiB*$^{-/-}$ mice. *In situ* hybridization and bright field microscopy were used to compare mRNA expression levels (black) of *Notch1* (**A–D**), *Hes1* (**E–H**) and *Hes5* (**I–L**) in E18.5 *NfiB*$^{+/+}$ (**A, B, E, F, I, J**) and *NfiB*$^{-/-}$ (**C, D, G, H, K, L**) brains. **A, C, E, G, I, K** Low magnification views; scale bar, 1000μm. **B, D, F, H, J** and **L** show boxed regions in **A, C, E, G, I** and **K**, respectively. Scale bar 500μm.

**Table 1**

List of abbreviations

| | |
|---|---|
| A | Anterior |
| BrdU | 5-Bromo-2-deoxyuridine |
| CC3 | Cleaved Caspase 3 |
| CP | Cortical plate |
| cpd | Cerebral peduncle |
| ctx | Cerebral cortex |
| DAPI | 4′,6-diamidino-2-phenylindole |
| DL-C | Region of deep layer (5–6) CTIP2+ neurons |
| DRAQ5 | 1,5-bis {[2-(Di-methylamino) ethyl]amino}-4, 8-dihydroxyanthracene-9, 10-dione |
| DP32 | DARPP32 antibody |
| E | Embryonic Day |
| GFP | Green Fluorescent Protein |
| L | Lateral |
| M | Medial |
| NFIB | Nuclear Factor One B |
| n.s. | not significant |
| oSVZ | Outer subventricular zone |
| o/SVZ | Region containing oSVZ and SVZ |
| P | Posterior |
| PLAP | Human placental alkaline phosphatase |
| po | pons |
| SEM | Standard error of means |
| SVZ | Subventricular zone |
| th | Thalamus |
| UL-S | Region of upper layer (2–4) SATB2+ neurons |
| VZ | Ventricular zone |
| WM | White Matter |

## Table 2

Summary of Primary Antibodies used for immunofluorescence (IF) in this study

| Antibody (clone) | Immunogen | Source (Catalog No.) | Host | Dilution |
|---|---|---|---|---|
| β-GAL | Purified full length native protein of *E. coli* β-Galactosidase | Abcam (ab9361) | Chicken (P) | 1:1000 |
| * BETA 3 (E-17) | Synthetic peptide to N-terminal amino acid residues ERGLHLGAAAASEDDLFLC of hamster BETA 3 (a.a. 4–22) | Santa Cruz Biotechnology (sc-6045) | Goat (P) | 1:100 |
| BrdU | Bromodeoxyuridine coupled to keyhole limpet hemocyanin (KLH) | Abcam (ab1893) | Sheep (P) | 1:250 |
| * Cleaved Caspase-3 | Synthetic peptide (KLH coupled) to N-terminal amino acid residues CRGTELDCGIETD of human Caspase-3 (a.a. 163–175) | Cell Signaling Technology (9661) | Rabbit (P) | 1:100 |
| * CTIP2 (25B6) | Fusion protein of amino acid residues MSRRKQG-NPQHLSQRELITPEADHVEAAILEEDEGLEIE-EPSGLGLMVGG of human CTIP2 (a.a. 1–50) | Abcam (ab18465) | Rat (M) | 1:750 |
| * DARPP32 (EP27Y) | N-terminal amino acid residues MLFRLSEHSSP-EEEASPHQRASGEGHHLKSKRPNPCAYTPPSL-KAVGRIA of human DARPP32 (a.a. 1–50) | Abcam (ab40801) | Rabbit (M) | 1:200 |
| GFP | Recombinant GFP protein emulsified in Freund's adjuvent | Aves Labs (GFP-1020) | Chicken (P) | 1:1000 |
| Ki67 (B56) | Immunodominant amino acid residues APKEKAQPLED-LASFQELSQ of human Ki67 (a.a. 2547–2566) | BD Pharmingen (550609) | Mouse (M) | 1:100 |
| NFIA | Amino acid residues PSTSPANRFVSVGPR of human NFIA (a.a. 478–492) | Active Motif (39397) | Rabbit (P) | 1:500 |
| NFIB | Amino acid residues PAPSSYFSHPTIRY of human NFIB (a.a. 402–415) | Active Motif (39091) | Rabbit (P) | 1:500 |
| * PAX6 | C-terminal amino acid residues QVPGSEPD-MSQYWPRLQ of mouse PAX6 (a.a. 420–436) | Covance (PRB-278P) | Rabbit (P) | 1:200 |
| PHH3 (6G3) | Synthetic phospho-peptide (KLH coupled) to amino acid residues ATKQTARKSTGGKA of human histone H3 (a.a. 2–15) | Cell Signaling Technology (9706) | Mouse (M) | 1:200 |
| SATB2 | Synthetic peptide (KLH coupled) to C-terminal amino acid residues ENDSEEGSEEMYKVEAEEENAD-KSKAAPAETDQR of mouse SATB2 (a.a. 700–733) | Abcam (ab34735) | Rabbit (P) | 1:1000 |
| * SOX2 (Y-17) | Synthetic peptide to C-terminal amino acid residues YLPGAEVPEPAAPSRLH of human SOX2 (a.a. 277–293) | Santa Cruz Biotechnology (sc-17320) | Goat (P) | 1:200 |
| * TBR1 | Synthetic peptide (KLH coupled) to amino acid residues SPLKKITRGMTNQSDTDNFPDSKDSPGDVQRSKLSPVLDG-VSELRHSFDGS of mouse TBR1 (a.a. 50–100) | Abcam (ab31940) | Rabbit (P) | 1:500 |
| * TBR2 | Synthetic peptide (KLH coupled) to acid residues STPSNGNSPPIKCEDINTEEYSKDTSKGMG-AYYAFYTSP of mouse TBR2 (a.a. 650–688) | Abcam (ab23345) | Rabbit (P) | 1:200 |
| Tuj1 | Raised against microtubules from rat brains | Covance (PRB-278P) | Mouse (M) | 1:1000 |

(P), polyclonal; (M), monoclonal

* Official and/or alternate gene names included in Antibody characterization of Material and Methods section.

**Table 3**

Functional Annotation Clustering of genes affected in E15.5 NfiB−/− mice

| Annotation Cluster | No. of genes | Enrichment score | GO_TERMS | p-value |
|---|---|---|---|---|
| 1 | 168 | 19.89 | cell cycle | 1.4E-26 |
| | | | M phase | 1.9E-22 |
| | | | cell division | 3.8E-20 |
| 2 | 123 | 15.61 | neuron differentiation | 3.7E-24 |
| | | | axonogenesis | 1.2E-16 |
| | | | axon guidance | 3.5E-13 |
| 3 | 100 | 16.64 | cell motion | 1.5E-15 |
| | | | neuron migration | 4.0E-10 |
| | | | localization of cell | 4.1E-09 |

**Table 4**

Signficantly changed expression of genes from Clusters 1–3

| Cluster | Gene Symbol | Gene Name | Fold change | p-value |
|---|---|---|---|---|
| 1 | Sycp3 | synaptonemal complex protein 3 | 6.080 | 1.01E-02 |
| | Id4 | inhibitor of DNA binding 4 | 2.257 | 2.08E-43 |
| | Gas1 | growth arrest specific 1 | 1.893 | 2.25E-28 |
| | Cenpe | centromere protein E | 1.488 | 1.62E-06 |
| | Cdca3 | cell division cycle associated 3 | 1.475 | 3.13E-09 |
| | Cdc14a | cell division cycle 14a | 1.452 | 8.42E-05 |
| | G0s2 | G0/G1 switch gene 2 | 0.402 | 6.16E-07 |
| | Trnp1 | TMF-regulated nuclear protein 1 | 0.553 | 2.26E-13 |
| | Rec8 | rec8 homolog | 0.616 | 5.55E-04 |
| 2 | Robo3 | roundabout homolog 3 | 5.898 | 5.54E-25 |
| | Neurog1 | neurogenin 1 | 2.476 | 7.01E-36 |
| | Gli3 | glioma 3 | 1.804 | 1.91E-21 |
| | Hes5 | hairy and enhancer of split 5 | 1.729 | 2.33E-18 |
| | Hes1 | hairy and enhancer of split 1 | 1.721 | 4.81E-13 |
| | Dll1 | delta like-1 | 1.646 | 4.69E-16 |
| | Notch3 | notch gene homolog 3 | 1.599 | 2.09E-12 |
| | Neurog2 | neurogenin 2 | 1.480 | 4.93E-12 |
| | Notch1 | notch gene homolog 1 | 1.205 | 1.16E-03 |
| | Lhx8 | LIM homeobox protein 8 | 0.147 | 1.34E-07 |
| | Nkx2-2 | NK2 transcription factor related, locus 2 | 0.174 | 7.40E-07 |
| | Isl1 | islet 1 transcription factor | 0.227 | 1.74E-35 |
| 3 | Mnx1 | motor neuron and pancreas homeobox 1 | 9.075 | 3.87E-16 |
| | Emx1 | empty spiracles homolog 2 | 1.653 | 2.08E-43 |
| | Smo | smoothened homolog | 1.415 | 8.31E-37 |
| | Nkx2-1 | NK2 homeobox 1 | 0.295 | 2.62E-09 |
| | Nkx2-3 | NK2 transcription factor related, locus 3 | 0.507 | 3.31E-06 |
| | Pou3f2 | POU domain, class 3, factor 2 | 0.547 | 1.03E-14 |

*J Comp Neurol*. Author manuscript; available in PMC 2014 June 15.

| Cluster | Gene Symbol | Gene Name | Fold change | p-value |
|---|---|---|---|---|
| | Cttnbp2 | cortactin binding protein 2 | 0.550 | 4.47E-20 |
| | Ntn1 | netrin 1 | 0.588 | 1.03E-08 |
| | Nrp1 | neuropilin 1 | 0.611 | 5.08E-04 |
| | Reln | reelin | 0.774 | 1.62E-04 |